THE UNIVERSITY OF READING

DEPARTMENT OF MATHEMATICS

The examination of balanced and unbalanced flow using Potential Vorticity in Atmospheric Modelling.

by M.A.Wlasak

Thesis submitted for the degree of

Doctor of Philosophy

January 2002

Abstract

Variational data assimilation (VAR) involves a minimisation of a cost functional with respect to a set of variables known as control variables. Within numerical weather prediction (NWP) VAR brings together observations and information from numerical models representing the atmosphere in a consistent way for a forecast to be made. It is considered desirable to define a set of control variables which separate the balanced and unbalanced parts of the flow. The current set of control variables used at the UK Met. Office represents the balanced control variable in terms of a streamfunction increment. Although this method is a good approw d V

Both the current Met Office method and the potential-vorticity-based method are implemented and tested numerically. The current method produces similar results to the potential vorticity method within high Burger regimes. This is due to the linearised potential vorticity increment approximating the vorticity in such regimes. Unlike the current method, however, the potential vorticity method is dependent on the Burger number and in low Burger regimes includes a substantial contribution from the height increment. The experiments suggest that the potential-vorticity-based method may be able to capture the balanced part of the flow better in low Burger regimes where the height increment is the balanced variable.

Acknowledgements

I wish to thank the many people whic

ontents

List of Figures

6.4 Full height incremen

List of Tables

hapter 1

Introduction

Mankind has attempted to predict the w

much potential energy present is that the possible motions which the atmosphere can exhibit are constrained. Large scale features are forced to move slowly with the quantities involved being in a sense '*balanced*' with respect to eac as a quantity summarising dynamical information that is present within a flow [28] such as frontogenesis, cyclogenesis and key features in general circulation. It has the distinctive property that it is conserved for inviscid, isentropic flow and as such can be used to track parcels of air. It also uses both rotational wind and pressure in its evaluation and describes better the balanced part of the flow in regions where variations in pressure are important.

In Chapter 2 the shallow water equations (SWEs) are derived with corresponding linearisations needed for an analytical examination needed of the system's dynamic properties. In Chapter 3 we examine the dynamical properties of the atmosphere within the context of the shallow water equations. In particular the concept of balance is systematically described. Within this chapter we show a number of issues already known within the literature but which tend to be forgotten. We show that the divergence tendency, as defined in Section 3.7, in general does not always filter the unbalanced aspects of the flow. Additional conditions need to be enforced. We show how a simple potential vorticity inversion model takes contributions from the height and the rotational wind in a way dependent on the flow regime.

In Chapter 4 we systematically present and discuss the choice of variables in which the data assimilation is performed. These variables are called *control variables*. We provide a framework in which different sets of control variables are discussed. Such a systematic appraisal of control variables is not present within the current literature. We take the method used presently by the UK Met. Office as an example and discuss the strength and weaknesses of the current change of control variables. The properties of an 'idealised' set of control variables are considered from a dynamical perspective using the dynamical background presented in the previous chapter.

We present various formulations of control variables based on potential vorticity, discussing their respective advantages and disadvantages and how they vary in different regimes. We finally develop a means of approximating the balanced parts of the unbalanced variables.

Chapter 5 gives the numerical techniques used to calculate the present choice of control variables used at the UK Met. Office. These techniques are used in experiments in Chapter 7. The chapter also presents a Fourier-based technique which is used in Chapter 6 to develop a means of obtaining the potential vorticity-based set of control variables. To the author's knowledge, the coupled system of equations has not been previously solved in this way. In both chapters validatory tests are performed. In Chapter 7, we present various experiments to compare potential vorticity based set of control variables with current method, which illustrate the theory given in previous chapters. Finally in Chapter 8 we summarise the findings and detail possible avenues for future work.

hapter 2

Shallow Water Equations

.1 Introduction

We first derive the shallow water equations (SWEs) on a rotating sphere from Newton's Second Law. This is necessary so as to give an accurate representation of the approximations made to obtain the equations, so that the results may be compared to other studies which use different approximations to the equations of motion on a rotating sphere. The discussion draws mainly on the treatments given by Pedlosky [43] and Randall [45] and includes the derivation of the incompressible three-dimensional Euler equations as a stepping stone to obtaining the shallow water equations.

We then present properties of the shallow water equations on a rotating sphere, linearised about two linearisation states: a resting state and a general time-invariant state. The former state is useful due to its idyllic simplicity while the latter state gives a template to derive other SWEs about more restrictive linearisations states necessary for the development of Chapters 3 and 6.

In addition, versions of the SWEs which approximate the spherical geometry are introduced. These versions, such as the β-plane approximation, are useful as a means of making analytical studies of the SWEs more tractable.

. Derivation of Shallow ater Equations on a Rotating Sphere from Newton's Second Law

Newton's Second Law of Motion states that the mass of an object multiplied by its absolute acceleration is equal to the total actual force acting on the object in a non-rotating co-ordinate system. When written for a fluid continuum, it is expressed in terms of density ρ, a three-dimensional wind $\mathbf{u}$, pressure p, the body force $\rho\nabla\phi$ and non-conservative force $\mathcal{F}$. In particular, ϕ is the potential field with which conservative body forces are represented and $\mathcal{F}$ is the frictional force. Newton's Second Law takes the form

$$\rho\frac{D\mathbf{u}}{Dt} = -\nabla p + \rho\nabla\phi + \mathcal{F}(\mathbf{u}), \tag{2.1}$$

where

$$\frac{D}{Dt} = \frac{\partial}{\partial t} + \mathbf{u}\cdot\nabla \tag{2.2}$$

is called the total material derivative with respect to time.

As stated, this law applies only on a stationary frame of reference. We wish to consider the momentum equation (2.1) for an observer in a uniformly rotating co-ordinate frame. We let the subscript I, represent a the non-rotating co-ordinate frame of reference and R are rotating one. We also denote the velocity under a rotating reference frame, $\mathbf{u}_R$, as the *relative velocity* and the velocity under a non-

where $\mathbf{A}$, $\mathbf{B}$, $\mathbf{C}$ are generic vectors. Thus,

$$\begin{aligned}
\boldsymbol{\Omega} \times (\boldsymbol{\Omega} \times \mathbf{r}) &= \boldsymbol{\Omega} \times (\boldsymbol{\Omega} \times \mathbf{r}_\perp) \\
&= (\boldsymbol{\Omega} \cdot \mathbf{r}_\perp)\,\boldsymbol{\Omega} - |\boldsymbol{\Omega}|^2 \mathbf{r}_\perp \\
&= 0 - \nabla \frac{|\boldsymbol{\Omega}|^2 |\mathbf{r}_\perp|^2}{2} \\
&= -\nabla \frac{|\boldsymbol{\Omega} \times \mathbf{r}_\perp|^2}{2}, \qquad (2.7)
\end{aligned}$$

since Ω and $\mathbf{r}_\perp$ are orthogonal.

We now incorporate the centripetal acceleration with the other conservative terms in (2.1) by defining the apparent gravitational potential,

$$\Theta = \phi + \frac{|\boldsymbol{\Omega} \times \mathbf{r}_\perp|^2}{2}. \qquad (2.8)$$

As the Coriolis acceleration $2\Omega \times \mathbf{u}_R$ cannot be further simplified, the momentum equation in a rotating co-ordinate frame is given by

$$\rho \left(\frac{D\mathbf{u}}{Dt} + 2\boldsymbol{\Omega} \times \mathbf{u} \right) = -\nabla p + \rho \nabla \Theta + \mathcal{F} \qquad (2.9)$$

where all $\mathbf{u}_R$ are written as $\mathbf{u}$.

So far we have not been specific as to the three-dimensional space we are considering. We define $\nabla\Theta$ to define the apparent vertical direction $\mathbf{k}^+$, which is perpendicular to an oblately spheroidal geopotential surface. However since the centripetal acceleration is very small compared to the constant body force $\nabla\phi$, we let $\nabla\Theta = \nabla\phi = g\mathbf{k}$, where $\mathbf{k}$ is a unit vector pointing radially away from the centre of a sphere and g is the acceleration due to gravity. The neglection of the centripetal acceleration allows the oblate spheroidal surface to be approximated by a spherical surface with unit vectors $\mathbf{i}, \mathbf{j}$ denoting longitude and latitude directions. The spherical latitude/longitude co-ordinate system is shown in Figure 2.1, where any

Figure 2.1: A sphere rotating at a constant angular velocity of magnitude Ω. The diagram also shows the direction of the orthonormal unit vectors $(\mathbf{i}, \mathbf{j}, \mathbf{k})$ for a spherical latitude θ, longitude λ co-ordinate system

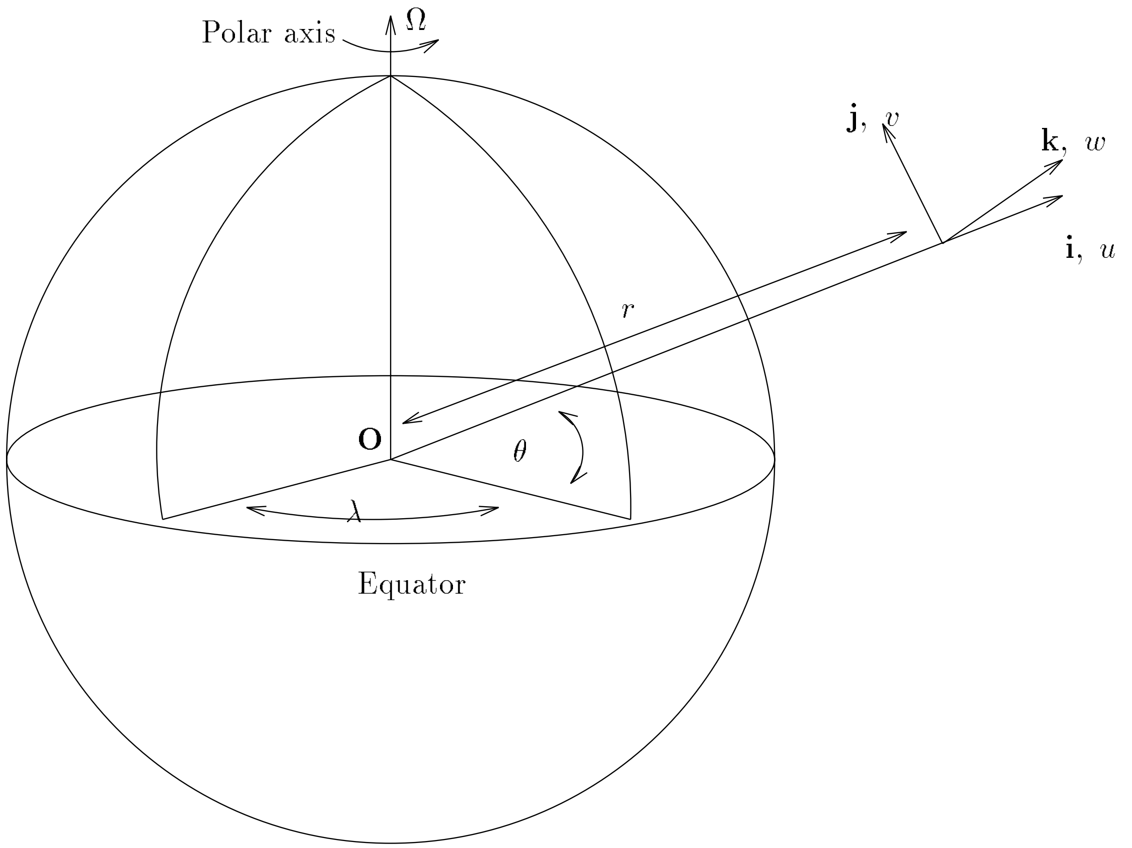

non-polar point in the three-dimensional space is either represented by $\lambda\mathbf{i} + \theta\mathbf{j} + r\mathbf{k}$ or more simply as (λ, θ, r). The three-dimensional wind in terms of its components is given by $\mathbf{u} = (u\mathbf{i} + v\mathbf{j} + w\mathbf{k})$. Although the co-ordinate system is degenerate at the poles, it is the natural choice for problems involving a spherical geometry.

Then, ignoring the effects of friction, the momentum equation becomes

$$\rho\left(\frac{D\mathbf{u}}{Dt} + 2\mathbf{\Omega} \times \mathbf{u}\right) = -\nabla p - \rho g\mathbf{k}. \tag{2.10}$$

For the following derivation of the SWEs we need the mass conservation equation. This equation is written as:

$$\frac{\partial \rho}{\partial t} + \text{‘ΨD!Ψ(”Tj!T‘T+}$$

We now simplify (2.10), (2.11) to get the shallow water equations on a rotating sphere. Let us write the pressure and density as

p

Let $h(\lambda, \theta, t)$ be the height at the free surface and $h_s(\lambda, \theta)$ represent the bottom topography

The momentum equation for the shallow water equations is derived by looking at the Coriolis, pressure gradient and the material derivative terms separately. Since we are considering a material derivative term on a surface, the material derivative term is simply $\frac{D\mathbf{v}}{Dt}$. As in equations (2.17), (2.18), the assumption of no vertical shear requires that there is no vertical advection to the horizontal momentum.

The pressure gradient term on the horizontal surface is obtained by integrating the hydrostatic equation (2.13) from some some arbitrary depth r within the fluid to the free surface h, giving

$$p(\lambda, \theta, h, t) - p(\lambda, \theta, r, t) = -g\rho(h - r), \tag{2.23}$$

with boundary conditions

$$p(\lambda, \theta, h, t) = p_f \qquad \text{and} \qquad p(\lambda, \theta, r, t) = g\rho\,(h - r) + p_f, \tag{2.24}$$

where p_f is the pressure at the free surface.

In equation (2.12) p is given in terms of a linearisation state $\overline{p}$ and perturbation p^*. Integration of the hydrostatic relation splits the pressure similarly, with

$$\overline{p} = -g\rho r \text{ and } p^* = g\rho h + p_f, \tag{2.25}$$

giving

$$\nabla p^* = g\rho\nabla h. \tag{2.26}$$

The $\mathbf{k}$ independen

Figure 2.2: A diagram representing the decomposition of vector $\mathbf{\Omega}$ into $\mathbf{j}$ and $\mathbf{k}$ components.

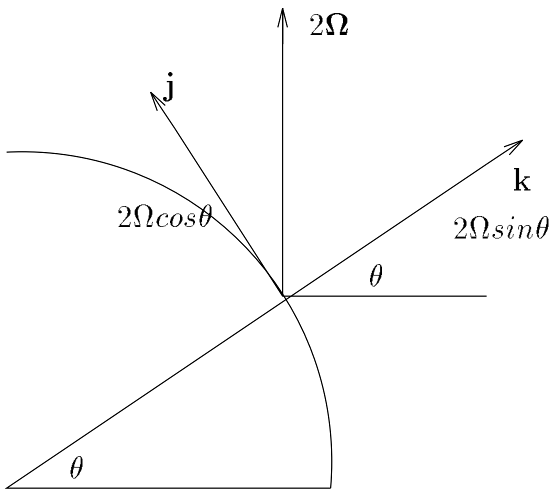

$$\begin{aligned} 2\mathbf{\Omega} \times \mathbf{u} &= (2\Omega \cos\theta \mathbf{j} + 2\Omega \sin\theta \mathbf{k}) \times \mathbf{u} \\ &= (2\Omega w \cos\theta - 2\Omega v \sin\theta)\,\mathbf{i} + (2\Omega u \sin\theta)\,\mathbf{j} + 2\Omega u \cos\theta \mathbf{k} \\ &= f\mathbf{k} \times \mathbf{v} + \textit{additional terms}. \end{aligned} \tag{2.27}$$

The additional terms are ignored; the $\mathbf{k}$ term is discarded because it violates the hydrostatic relation and does not lie on the spherical surface. The $2\Omega w \cos\theta \mathbf{i}$ is removed for consistent energy conservation to occur. This approximation is called the *traditional approximation* [17].

We now use (2.26) write the horizontal momentum equation as

$$\frac{D\mathbf{v}}{Dt} + f\mathbf{k} \times \mathbf{v} = -g\nabla h. \tag{2.28}$$

The advective part of the material derivative is not scalar invariant. The vector transformation $(\mathbf{v} \cdot \nabla)\,\mathbf{v} = \nabla\left[(\mathbf{v} \cdot \mathbf{v})/2\right] + (\nabla \times \mathbf{v}) \times \mathbf{v}$ is used to rewrite the momentum equation as

$$\frac{\partial \mathbf{v}}{\partial t} + \nabla\left[(\mathbf{v} \cdot \mathbf{v})/2\right] + (\nabla \times \mathbf{v}) \times \mathbf{v} + f\mathbf{k} \times \mathbf{v} \quad = \quad -g\nabla h$$

$$\Rightarrow \frac{\partial \mathbf{v}}{\partial t} + \nabla \left[\left(\mathbf{v} \cdot \mathbf{v} \right) / 2 \right] + \left(\left(\nabla \times \mathbf{v} \right) \cdot \mathbf{k} \right) \mathbf{k} \times \mathbf{v} + f \mathbf{k} \times \mathbf{v} = -g \nabla h$$

$$\Rightarrow \frac{\partial \mathbf{v}}{\partial t} + \nabla \left[\left(\mathbf{v} \cdot \mathbf{v} \right) / 2 \right] + (\zeta + f$$

rearranged, to give

$$\frac{\partial u}{\partial t} + \frac{u}{a\cos\theta}\frac{\partial u}{\partial \lambda} + \frac{v}{a}\frac{\partial u}{\partial \theta} - (f + \frac{u}{a}tan\theta)v$$

$$\frac{\partial v^*}{\partial t} + fu^* + \frac{g}{a}\frac{\partial h^*}{\partial \theta} = 0, \tag{2.40}$$

$$\frac{\partial h^*}{\partial t} + H\left(\frac{1}{a\cos\theta}\frac{\partial u^*}{\partial \lambda} + \frac{1}{a\cos\theta}\frac{\partial}{\partial \theta}(\cos\theta v^*)\right. = 0, \tag{2.41}$$

which are the shallow water equations linearised about a resting state and no bottom topography. The linearisation state for the height, H, has to be a constant, for the momentum equations to be consistent with the mass conservation equation.

We may rewrite the momentum equations in terms of vorticity and divergence. By applying the **k** component of the curl to the momentum equations we obtain the vorticity equation. It is given by

$$\frac{\partial \zeta^*}{\partial t} + f\zeta^* + \frac{2\Omega}{a}\cos\theta v^* = 0, \tag{2.42}$$

where the relative vorticity ζ^* is defined to be

$$\zeta^* = \frac{1}{a\cos\theta}\frac{\partial v^*}{\partial \lambda} - \frac{1}{a\cos\theta}\frac{\partial}{\partial \theta}(\cos\theta u^*). \tag{2.43}$$

In vector notation, the vorticity equation is written as

$$\frac{\partial \zeta^*}{\partial t} + \nabla\cdot(f\mathbf{v}^*) = 0, \tag{2.44}$$

where the divergence operator $\nabla\cdot$, and all subsequent spatial differential operators, lie on a spherical surface. The vector $\mathbf{v}^*$ denotes the wind on this surface and is equal to (u^*, v^*).

Application of the divergence operator to the momentum equations gives

$$\frac{\partial \delta^*}{\partial t} - f\zeta^* + 2\Omega\cos\theta u^* = -g\nabla^2 h^*, \tag{2.45}$$

where the divergence of the wind δ

The divergence equation can be written in terms of two scalar fields called the *streamfunction* ψ^* and *velocity potential* χ^*, which are defined through the relations:

$$\nabla^2\psi^* = \mathbf{k}\cdot\left(\nabla\times\mathbf{v}^*\right), \tag{2.47}$$

$$\nabla^2\chi^* = \nabla\cdot\mathbf{v}^*, \tag{2.48}$$

$$\mathbf{v}^* = \mathbf{k}\times\nabla\psi^* + \nabla\chi^*, \tag{2.49}$$

and has the form

$$\frac{\partial\delta^*}{\partial t} + \nabla f\cdot\left(\mathbf{k}\times\nabla\chi^*\right) - \nabla\cdot\left(f\nabla\psi^*\right) = -g\nabla^2 h^*, \tag{2.50}$$

where

$$\nabla f\cdot\left(\mathbf{k}\times\nabla\chi^*\right) = \frac{1}{a^2\cos\theta}\frac{\partial f}{\partial\theta}\frac{\partial\chi^*}{\partial\lambda}. \tag{2.51}$$

2.3.1 Potential Vorticity

We now consider the evolution of the potential vorticity q, w T Th eTy ć uT ΨΨ o t e‘n ȧ l times the linearised mass conservation equation (2.41), giving

$$\frac{Dq^*}{Dt} = \frac{1}{H}\left(\frac{\partial}{\partial t}\left(\zeta^* - \frac{f}{H}h^* \quad + \nabla \cdot (f\mathbf{v}^*) - f\nabla \cdot \mathbf{v}^* \quad = 0\right.\right. \tag{2.54}$$

and

$$\frac{\partial q^*}{\partial t} + (\mathbf{v}^* \cdot \nabla) \quad .)$$

tracting the linearisation state relations (2.57) and ignoring the quadratic perturbed terms. We obtain

$$\frac{\partial \mathbf{v}^*}{\partial t} + (\overline{\mathbf{v}}.\nabla)\,\mathbf{v}^* + (\mathbf{v}^*.\nabla)\,\overline{\mathbf{v}} + f\mathbf{k}\times\mathbf{v}^* \;=\; -g\nabla h^* \tag{2.58}$$

$$\frac{\partial h^*}{\partial t} + \nabla\cdot\left(\overline{h}\mathbf{v}^* + h^*\overline{\mathbf{v}}\right) \;=\; 0. \tag{2.59}$$

2.4.1 Vorticity and Divergence Equations

The vorticity equation and divergence equations are just generalisations of (2.42) and (2.46). The vorticity equation is

$$\frac{\partial \zeta^*}{\partial t} + \nabla\cdot\left(\left(\overline{\zeta} + f\right)\mathbf{v}^* + \zeta^*\overline{\mathbf{v}}\right) \;=\; 0, \tag{2.60}$$

while the divergence equation is$iTD/Tc/\delta\zeta Tj/TTf/TD/Tc/\lambda Tj/\quad T/q/cm/ImDo/Q/BT/TTf/TmiTc$

The potential vorticity increment q^* associated with this linearisation state is

$$\frac{q^*}{\overline{q}} = \frac{\zeta^*}{\overline{\zeta} + f} - \frac{h^*}{\overline{h}} + \mathcal{O}((h^*)^2, h^*\nabla \times \mathbf{v}^*, (\nabla \times \mathbf{v}^*)^2). \tag{2.64}$$

where ζ^*, $\overline{\zeta}$ are defined b

$$y = a\left(\theta - \right.$$

$$\frac{\partial \delta^*}{\partial t} + u^+ \frac{\partial \delta^*}{\partial x} - (f_0 + \beta y) \left(\frac{\partial v^*}{\partial x} - \frac{\partial u^*}{\partial y} \right. + \beta u^* + g \left(\frac{\partial^2 h^*}{\partial x^2} + \frac{\partial^2 h^*}{\partial y^2} \right. = 0, \quad (2.69)$$

$$\frac{\partial h^*}{\partial t} + u^+ \frac{\partial h^*}{\partial x} + H \left(\frac{\partial u^*}{\partial x} + \frac{\partial v^*}{\partial y} \right. = 0. \quad (2.70)$$

These equations in streamfunction and velocity potential formulation are

$$\left(\frac{\partial}{\partial t} + u^+ \frac{\partial}{\partial x} \right. \nabla^2 \psi^* + (f_0 + \beta y) \nabla^2 \chi^* + \beta \left(\frac{\partial \psi^*}{\partial x} + \frac{\partial \chi^*}{\partial y} \right. = 0, \quad (2.71)$$

$$\left(\partial \right.$$

.6 hy Shallow ater Equations?

As shown in the derivation in Section 2.2, the SWEs assume there is no vertical shear and that the implied vertical velocity is given by equation (2.17). Such an approximation assumes that the fluid is *shallow* with the range of heights considered being small compared to wavelengths in the horizontal direction. It also expects the fluid to have weak vertical motion. The lack of vertical shear is the most serious limitation of the SWEs as an atmospheric model.

The SWEs are not a viable atmospheric model as it has far too many limitations to its behaviour. Even so, the SWEs on a rotating sphere have many dynamical mechanisms which are revelent to the more general problem. The spherical geometry has in itself made interesting features with quite specialised boundary conditions. The effects of a rotating sphere are considered by a variable Coriolis term f. The SWEs exhibit non-trivial solutions due their nonlinearity in the advective term and have slow and fast aspects to the flow which behave very differently from each other. These properties are examined in the following chapter, where the concepts of *balance* and *geostrophic adjustment* are introduced.

hapter 3

Dynamical ehaviour of the SWEs

3.1 Introduction

In Chapter 2 we derived the SWEs. We now present the dynamical heart of the SWEs. In particular we present the concepts of characteristic scales and regimes in Section 3.2, wave solutions, balance in Section 3.3 and geostrophic adjustment in Section 3.6. We show that divergence tendency, as defined in Section 3.7, in general does not always filter the 'noise' aspects of the flow: additional conditions also need to be established. We present an example of a wave 'in balance' - the Rossby–Haurwitz wave in Section 3.4. We examine the departure from linear balance and the divergence and show that dynamically, for a simplified problem, they are propagated by a linear combination of the eigenmodes of the dynamical system. We then finally look at in Section 3.9 the behaviour of perturbations satisfying a linear balance relationship and linearised potential vorticity under different Burger regimes.

3. Characteristic Scales, Regimes: Rossby and Burger numbers

Atmospheric dynamics typically involve an interaction of waves with various wavelengths and amplitudes. A technique to identify the relative importance of one term in a set of equations over another is to non-dimensionalise the problem and assume that the flow is characterised by a typical velocity U and typical height H. We assume that the height and winds are harmonic and the flow is identified by a single typical wavelength λ. The characteristic horizontal length scale L is then equal to $L = \lambda/(2\pi)$ [16]. The corresponding time-scale for the height and wind fields is set to L/U.

Using the scaling defined above the non-dimensional quantities, denoted by $\breve{}$, are

$$\begin{aligned} \mathbf{v} &= U\breve{\mathbf{v}}, \\ h &= H\breve{h}, \\ (\lambda, \theta, t) &= \left(L\breve{\lambda}, L\breve{\theta}, \frac{L}{U}\breve{t}\right) \end{aligned} \tag{3.1}$$

where h, $\mathbf{v}$ are the height and wind fields on the spherical surface, defined at the end of Section 2.2. The latitude, longitude co-ordinates are given by λ, θ and t denotes the time.

Introducing equations (3.1) into the momentum equation part of the full non-linear SWE on the rotating sphere (2.29) gives

$$\frac{U^2}{L}\left(\frac{\partial \breve{\mathbf{v}}}{\partial \breve{t}} + \nabla\left[\left(\breve{\mathbf{v}} \cdot \breve{\mathbf{v}}\right)/2\right] + \left(\nabla \times \breve{\mathbf{v}}\right) \times \breve{\mathbf{v}}\right. + fU\mathbf{k} \times \breve{\mathbf{v}} = -\frac{gH}{L}\nabla \breve{h}. \tag{3.2}$$

where, for this section, the vector operators are applied to scaled $\left(\breve{\lambda}, \breve{\theta}, \breve{t}\right)$.

Dividing equation (3.2) by fU gives

$$
\begin{aligned}
\frac{U}{fL}\left(\frac{\partial \breve{\mathbf{v}}}{\partial t} + \nabla\left[\left(\breve{\mathbf{v}}\cdot\breve{\mathbf{v}}\right)/2\right] + \left(\nabla\times\breve{\mathbf{v}}\right)\times\breve{\mathbf{v}}\right. & \\
+\mathbf{k}\times\breve{\mathbf{v}} &= -\frac{gH}{fUL}\nabla\breve{h}, \quad - \\
\Rightarrow \frac{U}{fL}\left(\frac{\partial \breve{\mathbf{v}}}{\partial t} + \nabla\left[\left(\breve{\mathbf{v}}\cdot\breve{\mathbf{v}}\right)/2\right] + \left(\nabla\times\breve{\mathbf{v}}\right)\times\breve{\mathbf{v}}\right. & \\
+\mathbf{k}\times\breve{\mathbf{v}} &= -\left(\frac{gH}{f^2L^2}\right.\left(\frac{fL}{U}\right.\nabla\breve{h}, \quad (3.3)
\end{aligned}
$$

which by setting the non-dimensional numbers

$$
R_o = \frac{U}{fL},
$$

magnitude than the velocity $\check{\mathbf{v}}$. The consequences of this are examined in Sections 3.6 and 3.9.

The three-dimensional atmosphere tends to have large horizontal length scales and relatively small vertical length scales and can be approximated by being considered as a number of layers of fluid on top of each other. A fluid with this property is said to be stably stratified. The Burger number describes the relative importance of the effects of stratification and rotation. When this number is larger than one the layers are stable with respect to changes in the interfaces between them ; for Burger number much smaller than one the rotation dominates the flow.

The Burger number is described in numerous ways dependent on the source. Pedlosky [43] defines for two-dimensional horizontal flow the non-dimensional number as $gH/(f^2L^2)$, the square of the quantity described here. Haltiner et al. [23] defines the Burger number as the ratio between the the Rossby radius of deformation, defined as

$$L_r = \frac{\sqrt{gH}}{f} \tag{3.9}$$

and the characteristic length scale L, which is identical to the definition given in equation (3.5).

As described in Chapter 2, the SWEs are defined on a two-dimensional surface and consist of a single layer of fluid. A non-trivial interface is considered whet‘!‘Tc!Ψw”igpeΨflu

obtain

$$\left[\left(n_1\left(\frac{\partial}{\partial t}\nabla^2+u^+\frac{\partial}{\partial x}\nabla^2+\beta\frac{\partial}{\partial x}\right.^2+f_0^2\nabla^4\right)\left(\frac{\partial}{\partial t}+u^+\frac{\partial}{\partial x}\right.\right.$$
$$\left.-\,gH\left(\frac{\partial}{\partial t}\nabla^2+u^+\frac{\partial}{\partial x}\nabla^2+\beta\frac{\partial}{\partial x}\quad\nabla^4\right]h^* \quad=\quad 0.(3.11)$$

We assume that the height perturbations have a harmonic structure

$$h^*=\hat{h}e^{i(k_1x+k_2y-\sigma t)} \tag{3.12}$$

where $\hat{h}$ is a complex coefficient associated with the both wavenumbers, k_1 and k_2, and the angular frequency σ. The symbol i denotes the imaginary number satisfying $i^2=-1$. Introducing (3.12) into (3.11), produces a cubic polynomial in σ

$$\left[f_0^2K^4-n_1\left(\sigma K^2-u^+k_1K^2+\beta k_1\right)^2\right]\left(-i\sigma+u^+ik_1\right)$$
$$-gH\left(i\sigma K^2-u^+ik_1K^2+\beta ik_1\right)K^4 \quad=\quad 0$$
$$\Rightarrow\left[f_0^2K^4-n_1\left(\sigma K^2-u^+k_1K^2+\beta k_1\right)^2\right]\left(\sigma-u^+k_1\right)$$
$$+gH\left(\sigma K^2-u^+k_1K^2\right.$$

[A dispersion relation for the β-plane can be obtained by retaining the β terms in (3.13), and solving the resulting cubic using Vieta's subsitution [57]. We leave such details as they serve as a distraction to the discussion given.]

The smallest root is approximated by setting the tracer n_1 to zero. In this situation, the cubic polynomial (3.13) reduces to a linear equation in σ, where

$$\sigma = k_1 u^+ - \frac{gH\beta k_1}{gHK^2 + f_0^2} = k_1 u^+ - \frac{\beta k_1}{K^2 + \frac{f_0^2}{gH}}. \tag{3.15}$$

The dispersion relation (3.15) defines the angular frequency of what is identified as a *Rossby wave.*

Setting the tracer n_1 to zero is equivalent to setting the total material time derivative term and $\beta\frac{\partial\chi}{\partial x}$ of the divergence equation (2.76) to zero. As observed in [55], the condition that is necessary and sufficient for the elimination of inertio-gravity waves of the form (3.14) requires $\left(\sigma K^2 - u^+ k_1 K^2 + \beta k_1\right)^2 = 0$. However it is necessary for the existence of solutions of the type (3.15) that $(\sigma K^2 - u^+ k_1 K^2 + \beta k_1)$ does not vanish, justifying the need to set the tracer to zero. This is called the *generalised filtering approximation.* The remaining part of the divergence equation is given by the linear balance equation,

$$\nabla \cdot f_0 \nabla \psi = g\nabla^2 h. \tag{3.16}$$

The main balance relation used in this thesis resembles (3.16). However, we generally consider a spherical domain and allow the Coriolis parameter f to vary with latitude. The resulting equation (3.37) is described in Section 3.5 and in Chapter 4.

When the inertio-gravity waves are no longer present, the fluid is considered to be in *balance.* This occurs when the dispersion relations related to the two largest roots of the cubic equation (3.13) are not exhibited by the flow in question; the motion of the fluid only is described by the dispersion relation defined by the smallest root of the frequency equation. Models which propagate only Rossby waves are called *balanced models*. There are a number of techniques to approximate balance and produce balanced models, obtained from using semi-geostrophic or quasi-geostrophic theories [21]. They all share the property that provided we consider linearised SWEs with constant coefficients, the dispersion relation defined by the smallest root of the SWEs cubic frequency equation is equivalent to the linear dispersion relation of the respective balanced model.

Typically, in a mid-latitude region the characteristic height H is approximately equal to 10 km with the inertio-gravity waves and Rossby waves having speeds around $300ms^{-1}$ and $10ms^{-1}$, respectively. This shows the large separation in timescales between the two types within the mid-latitudes. Pairs of inertio-gravity waves with same angular frequency and amplitude move in opposite directions to each other. The Rossby wave propagates westwards which is in the direction perpendicular to the potential vorticity gradient relative to the mean flow.

Given the low angular frequency of the Rossby wave, the wave phase speed is expected to be slow. This is true for linearised equations. However, when the nonlinear advective term $(\mathbf{v} \cdot \nabla)\,\mathbf{v}$ is present, slow Rossby waves interact with each other to give waves that are slower or faster. Instead of there being a clear distinction between the timescales of fast inertio-gravity waves and slow Rossby waves, the nonlinear interactions produce Rossby waves with a wide range of angular frequencies. The amplitude and energy present within these waves diminish with increased angular frequency. However in a non-linear description of balanced flow all Rossby waves need to be considered. Potential vorticity is a good variable to choose in this respect

compared to the magnitude of the height field H itself. We now present a derivation of a Rossby–Haurwitz wave, similar to the treatment given by Dutton [16].

If the waves are assumed to propagate only in the x direction, we can let the solutions take the form

$$
\begin{aligned}
u &= \hat{u} e^{(k_1 x - \sigma t) i}, && (3.20) \\
v &= \hat{v} e^{(k_1 x - \sigma t) i}, && (3.21) \\
h &= \hat{h} e^{(k_1 x - \sigma t) i}, && (3.22)
\end{aligned}
$$

and substitute (3.20)-(3.22) into (3.17)-(3.19), to obtain

$$
\begin{aligned}
i\left(-\sigma + k_1 u^+\right)\hat{u} - (f_0 + \beta y)\hat{v} + igk_1\hat{h} &= 0 && (3.23) \\
i\left(-\sigma + k_1 u^+\right)\hat{v} + (f_0 + \beta y)\hat{u} + g\frac{\partial \hat{h}}{}
\end{aligned}
$$

where C_1, C_2 are constants which are fixed by appropriate boundary conditions. If the boundary conditions are such that the domain considered is a channel of width D for which $|\hat{v}|$ is at a maximum at $y = 0$ and zeros at $y = \pm D/2$, then

$$\begin{aligned} C_2 &= 0 \\ \left(\frac{\beta}{u^+ - \frac{\sigma}{k_1}} - k_1^2\right)^{\frac{1}{2}} \frac{D}{2} &= \frac{\pi l}{2} \quad \text{for} \quad l = \pm 1, \pm 3, \ldots \quad . \end{aligned} \tag{3.29}$$

The dispersion relation is obtained by rearranging (3.29) into

$$\sigma = k_1 u^+ - \frac{\beta k_1}{k_1^2 + \left(\frac{l\pi}{D}\right)^2}. \tag{3.30}$$

The relationship between the Rossby wave within the SWEs and the Rossby–Haurwitz wave under two-dimensional Euler equations are readily seen by letting $H \to \infty$ in (3.15) and $D \to \infty$ in (3.30). In both situations, the t‘cm!f!“TD!ΨH”Tj!T“Tf!“T

Solving this Monge-Ampere equation provides the appropriate balanced height. It is important to note that the Rossby–Haurwitz wave in SWEs context does not produce a balanced flow that stays balanced when propagated in time. At best, under a high Burger regime, the Rossby–Haurwitz wave produces SWEs solutions over 12 hours with relatively little divergence [6] which are close to the balanced flow given by the two-dimensional Euler equations. As such, it is used as an initial solution which produces solutions over a $12hrs - 24hrs$ timescale that is close to balance.

3.4.1 The Rossby–Haurwitz wave on a Sphere

In practice, throughout this thesis the initial height and wind field relating to a Rossby–Haurwitz wave is defined over a sphere [44]. This wave is characterised by parameters a, g, Ω, R, h

where the variables $A(\theta),\ B(\theta),\ C(\theta)$ are given by

$$\begin{aligned}
A(\theta) &= \frac{\omega}{2}(2\Omega+\omega)\cos^2\theta + \frac{1}{4}K^2\cos^{2R}\theta[(R+1)\cos^2\theta \\
&\quad +(2R^2-R-2) - 2R^2\cos^{-2}\theta], \\
B(\theta) &= \frac{2(\Omega+\omega)K}{(R+1)(R+2)}\cos^R\theta[(R^2+2R+2) \\
&\quad -(R+1)^2\cos^2\theta], \\
C(\theta) &= \frac{1}{4}K^2\cos^{2R}\theta[(R+1)\cos^2\theta-(R+2)].
\end{aligned} \tag{3.36}$$

3.5 Linear Balance Equation

In Section 3.3 we derived the linear balance equation (LBE) by applying the general filtering approximation to SWEs defined on a Cartesian mid-latitude β-plane (2.73), (2.75) and (2.76). More generally LBE is defined over the sphere, where

$$g\nabla^2 h - \nabla\cdot f\nabla\psi = 0 \tag{3.37}$$

and ψ, the streamfunction is defined by (2.47). In subsequent chapters this balance relation is compared with another which conserves potential vorticity. Consequently, the properties of this balance condition need to be described.

The LBE is viewed in more than one way. Burger [7] considers the LBE as a simple generalisation of geostrophic balance over the whole sphere for waves of planetary length scale $L \approx a$. By applying scaling arguments with this length scale to the divergence equation (2.61) about mid-latitudes, the terms in (3.37) are found to be ten times larger than the other terms in the divergence equation.

It is also a linear non-divergent mass-wind law that naturally takes into account the latitudinal variation of the Coriolis parameter and is useful when length scales

$L \approx 10^6 m$ are considered [12]. However, balanced divergent parts to a wind do exist for the SWEs on a sphere [49] and are 'invisible' to this balance condition. This is seen when appropriate equations are added to LBE to produce a closed energically-consistent dynamical system [58]. This requires not only a modified vorticity equation but also a thermodynamic equation. The kinetic energy of this particular dynamical system comes from only the rotational part of the flow and no divergent contribution exists.

Two problems need to be considered: the calculation of a balanced height field from the streamfunction

$$g\nabla^2 h = \nabla \cdot f \nabla \psi \tag{3.38}$$

and the backward relation

$$\nabla \cdot f \nabla \psi = g \nabla^2 h \tag{3.39}$$

where the streamfunction is determined by the height.

The calculation of a balanced height field from the streamfunction is straightforward; the existence, uniqueness and boundary conditions are the same as those needed to invert a Poisson equation on a sphere and are given in Section 5.5.

The reverse transformation, the transformation from height field to a streamfunction, is a little more complex. The majority of the attempts to solve (3.39) set the problem in terms of spherical harmonics [37], [1]. Daley [14] shows that solutions to the reverse transformation can become singular about the equator. The problem is worsened by the sensitivity of the solution to the height field localised about the equator; small errors in the heightithT“TfrrjGΨin”sΨby!Ψfl”Tj!Trk”ΨerjGΨin”Ψ3;”ΨsΨThe”lΨs

In [12] Daley considers the practical use of (3.39) with height fields including error and shows that the solution tends to be erroneous within 20 degrees latitude of the equator. A means to get around this difficulty is to modify the linear balance equation so that these singularities do not exist [14] using an approach that uses the singular value decomposition method. This procedure has the effect of making the reverse LBE as accurate as the forward LBE outside the tropics as well as removing possible singularies in the streamfunction around the equator. A consequence of these considerations is that the reverse transformation is not used.

3.6 Geostrophic Balance and Geostrophic Adjustment

In Section 3.2, we showed that when R_o

3.7 Divergence Tendency

A justification for using the Charney balance condition to derive a balanced height field as an initial condition for the SWEs is due to the observation that introducing a purely rotational wind into the divergence equation sets the local change in the divergent wind, the *divergence tendency* $\partial\nabla^2\chi/\partial t$, to be zero [8].

Let us consider SWEs linearised about a resting state on an f-plane. The setting of the divergence tendency to zero reduces the cubic frequency equation to a linear one and gives the dispersion relationship for the balanced fields. In this situation the inertio-gravity waves are fully filtered out of the system. The divergence equation reduces to (3.16). However when the SWEs are linearised about a constant velocity u^+ and a β-plane approximation is used, setting the divergence tendency to zero only reduces the cubic frequency equation to a quadratic; the different linearisation state gives a set of perturbed equations which no longer have the symmetry that exists in the f-plane case and the inertio-gravity waves are no longer fully filtered.

We can see this again, by considering an f-plane model of the SWEs, linearised about a resting state

$$\frac{\partial\zeta}{\partial t} + f_0\delta = 0 \tag{3.44}$$

$$\frac{\partial\delta}{\partial t} - f_0\zeta = -g\nabla^2 h \tag{3.45}$$

$$\frac{\partial h}{\partial t} + H\delta = 0 \tag{3.46}$$

$$\tag{3.47}$$

where f_0 and H are constant values. Setting the partial time derivative $\frac{\partial\delta}{\partial t}$ to zero, enforces the divergence δ to be constant. If we take the remaining terms of the divergence equation and apply the partial time derivative operator we get

$$
\begin{aligned}
f_0 \frac{\partial \zeta}{\partial t} - g \frac{\partial \nabla^2 h}{\partial t} &= 0 && (3.48) \\
\Rightarrow gH\nabla^2 \delta - f_0^2 \delta &= 0, && (3.49)
\end{aligned}
$$

substituting the partial time derivative for the divergence using the vorticity and continuit

We apply the spatial Fourier decomposition

$$\hat{\boldsymbol{X}} = \begin{pmatrix} \hat{u}_{k_1,k_2}(t) \\ \\ \hat{v}_{k_1,k_2}(t) \\ \\ \hat{h}_{k_1,k_2}(t) \end{pmatrix} = \int_{y=-\infty}^{y=\infty} \int_{x=-\infty}^{x=\infty} \begin{pmatrix} u^*(x,y,t) \\ \\ v^*(x,y,t) \\ \\ h^*(x,y,t) \end{pmatrix} e^{-i(k_1 x + k_2 y)}\, dxdy, \tag{3.51}$$

in the xy plane to transform the coupled system of PDE's into a coupled system of ODE's which for each k_1, k_2 is represented by

$$\hat{\boldsymbol{X}}_t + L\hat{\boldsymbol{X}} = 0, \tag{3.52}$$

with

$$L = \begin{pmatrix} 0 & -f_0 & igk_1 \\ \\ f_0 & 0 & igk_2 \\ \\ iHk_1 & iHk_2 & 0 \end{pmatrix}. \tag{3.53}$$

We now calculate the eigenvalues and eigenvectors of the system. The determinant of the characteristic equation is given by

$$det\, |L - i\lambda_+ I| = i\lambda_+ \left(\lambda_+^2 + \sigma^2\right), \tag{3.54}$$

where $\lambda_+ = (O, -\sigma, \sigma)$,$\sigma = (f_0^2 + gHK_w^2)^{\frac{1}{2}}$ and $K_w^2 = k_1^2 + k_2^2$. The eigenvalues $i\Lambda$ and eigenvectors $\quad = (\boldsymbol{e}_1, \boldsymbol{e}_2, \boldsymbol{e}_3)$ are related by

$$L \quad = i \quad \Lambda \tag{3.55}$$

with

$$= (\boldsymbol{e}_1\ \boldsymbol{e}_2\ \boldsymbol{e}_3) = \begin{pmatrix} igk_2 & -igk_1 - \frac{gk_2 f}{\sigma} & \frac{gk_2 f}{\sigma} \\ \\ igk_1 & -igk_2 + \frac{gk_1 f}{\sigma} & -igk_2 - \frac{gk_1 f}{\sigma} \\ \\ f & i\left(\sigma - \frac{f^2}{\sigma}\right) & -i\left(\sigma - \frac{f^2}{\sigma}\right) \end{pmatrix} \tag{3.56}$$

and

$$\Lambda = \begin{pmatrix} 0 & 0 & 0 \\ 0 & -\sigma & 0 \\ 0 & 0 & \sigma \end{pmatrix}. \tag{3.57}$$

The inverse of the matrix of eigenvectors, $^{-1}$, is given by

$$^{-1} = \begin{pmatrix} \boldsymbol{f}_1 \\ \boldsymbol{f}_2 \\ \boldsymbol{f}_3 \end{pmatrix} = \frac{g}{2i\sigma g^2 K_w^2} \begin{pmatrix} -\frac{2gHk_1K_w^2}{\sigma} & \frac{2gHk_1K_w^2}{\sigma} & \frac{2igfK_w^2}{\sigma} \\ -k_1\sigma - ik_2 f & -k_2\sigma + ik_1 f & gK_w \\ -k_1\sigma + ik_2 f & -k_2\sigma - ik_1 f & -gK_w \end{pmatrix} \tag{3.58}$$

and is calculated by taking the complex conjugate of the matrix of co-factors of ,

divided by the determinant of .

Now we are in a position to apply a similarity transformation to uncouple the

system Tj!‘‘TD!j!T‘inAned.Ψa”Let‘‘TD!‘Tc!ΨE.”Tj!Tc!ΨNo”Tj!‘‘TD!D!Ψ!”Tj!T‘j!7‘TD!Ψf”Tj‘‘j!Y‘‘

are given by

$$
\begin{aligned}
\hat{y}^{(1)}_{k_1,k_2}(t) &= \hat{y}^{(1)}_{k_1,k_2}(0), \\
\hat{y}^{(2)}_{k_1,k_2}(t) &= e^{-i\sigma t}\hat{y}^{(2)}_{k_1,k_2}(0), \\
\hat{y}^{(3)}_{k_1,k_2}(t) &= e^{i\sigma t}\hat{y}^{(3)}_{k_1,k_2}(0).
\end{aligned}
\tag{3.68}
$$

Since $\hat{\boldsymbol{Z}} = BP\hat{\boldsymbol{Y}}$

3.9 Relative Contributions to Scaled Potential Vorticity Perturbations

We now consider properties of height, vorticity and potential vorticity perturbations that satisfy both the linearised potential vorticity relationship (3.64) and the linear balance equation (3.16) when the Coriolis term f_0 is constant. It is valid to consider relative vorticity perturbations ζ_{rel}^* since the linear balance equation (3.16) for constant f_0 is equal to

$$f_0 \zeta_{rel}^* = g \nabla^2 h^*. \tag{3.70}$$

We describe how the ratio between scaled perturbations in height and absolute vorticity changes with the Burger number. The change in this ratio is equivalent to a change in the relative contribution of these terms as needed to produce scaled potential vorticity peturbations. This is because the scaled potential vorticity perturbation is defined to be the sum of the scaled perturbations in height and absolute vorticity. To show this mathematically, we define perturbations of any quantity, as in Chapter 2, to be the difference between the true value and its respective linearisation state. By letting perturbations satisfy both the linearised potential vorticity equation and the linear balance equation (3.70), an equation is found that shows how the potential and absolute vorticity perturbations are inextricably linked to the Burger number. Next, we present an equation that links the potential vorticity perturbation to both the height perturbation and the Burger number.

Let us first consider the velocity and height to be on a two dimension Cartesian grid with standard axes (x, y). Suppose that both the linearisation states and the perturbations in the velocity and height are known. The relative vorticity linearisation state $\overline{\zeta_{rel}}$ and the relative vorticity ζ^*_{rel} perturbation are calculated using

$$\overline{\zeta_{rel}} = \frac{\partial \overline{v}}{\partial x} - \frac{\partial \overline{u}}{\partial y}, \qquad \zeta^*_{rel} = \frac{\partial v^*}{\partial x} - \frac{\partial u^*}{\partial y}. \tag{3.71}$$

The full nonlinear potential vorticity q and linearisation state $\overline{q}$ are defined as

$$q = \frac{1}{h}\left(\frac{\partial v}{\partial x} - \frac{\partial u}{\partial y} + f_0\right) \equiv \frac{\zeta_{rel} + f_0}{h} \tag{3.72}$$

$$\overline{q} = \frac{1}{\overline{h}}\left(\frac{\partial \overline{v}}{\partial x} - \frac{\partial \overline{u}}{\partial y} + f_0\right) \equiv \frac{\overline{\zeta_{rel}} + f_0}{\overline{h}}, \tag{3.73}$$

where (3.73) is the Cartesian f-plane form of (2.63). By linearising the nonlinear potential vorticity equation (3.72), the perturbations in potential vorticity q^*, height h^* and absolute vorticity ζ^*_{rel} are connected by the equation

$$\frac{q^*}{\overline{q}} = \frac{\zeta^*_{rel}}{\overline{\zeta_{rel}} + f_0} - \frac{h^*}{\overline{h}}. \tag{3.74}$$

We use the relationship (3.70) between the perturbation in absolute vorticity and the height to derive a relationship between the potential vorticity perturbation and the height. We consider perturbations in the height and the velocity that take the form $h^* = \hat{h}e^{i(k_1x+k_2y-\sigma t)}$, $u^* = \hat{u}e^{i(k_1x+k_2y-\sigma t)}$, $v^* = \hat{v}e^{i(k_1x+k_2y-\sigma t)}$

can be determined: one defines scaled perturbations in potential vorticity in terms of scaled perturbations in height, the other shows how perturbations in scaled relative vorticity perturbations are related to scaled perturbations in potential vorticity. These relationships are given by

$$\frac{q^*}{\overline{q}} = -N\frac{h^*}{\overline{h}} \qquad \left(1 - \frac{1}{N}\right)\frac{q^*}{\overline{q}} = \frac{\zeta^*_{rel}}{\overline{\zeta_{rel}} + f_0} \tag{3.76}$$

with

$$N = 1 + \frac{f_0\ B_u^2}{\overline{\zeta_{rel}} + f_0}. \tag{3.77}$$

As the Burger number is always greater than zero, for any given perturbation, N is always greater than 1. For a fixed $q^*/\overline{q}$ and $N >> 1$, $h^*/\overline{h}$ will not contribute much to the scaled potential vorticity perturbations; the potential vorticity perturbations are sensitive to the absolute vorticity perturbations with $q^*/\overline{q} \ \approx \zeta^*_{rel}/(\overline{\zeta_{rel}} + f_0)$. Moreover, the greater the value of N, the more sensitive $q^*/\overline{q}$ will be to $\zeta^*_{rel}/(\overline{\zeta_{rel}}+f_0)$. The equation (3.77) shows that a number of conditions can make N large. One possible way, assuming $(\overline{\zeta_{rel}} + f_0)$ to be constant, is to produce a large Burger number. A large Burger number will be obtained when $\overline{h}$ is large or when f_0 is small. In summary, it is expected that for large Burger number $q^*/\overline{q}$ will be dominated by changes in $\zeta^*_{rel}/(\overline{\zeta_{rel}} + f_0)$. The equations (3.76) and (3.77) can also be written as

$$\left(1 - \frac{1}{P}\right)\frac{q^*}{\overline{q}} = -\frac{h^*}{\overline{h}} \qquad \frac{q^*}{\overline{q}} = P\frac{\zeta^*_{rel}}{\overline{\zeta_{rel}} + f_0} \tag{3.78}$$

with

$$P = 1 + \frac{\overline{\zeta_{rel}} + f_0}{f_0 B_u^2}. \tag{3.79}$$

It is clear that for a small Burger number, $P >> 1$ with $q^*/\overline{q} >> \zeta^*_{rel}/(\overline{\zeta_{rel}} + f_0)$ and $q'/\overline{q} \approx h'/\overline{h}$. In this situation it is the scaled height perturbations $h'/\overline{h}$

which will dominate $q'/\overline{q}$. Small Burger number regimes will occur where f_0 is not small as in the mid-latitudes and where $\overline{h}$ is small. It is in these regions that the height perturbations will most resemble the potential vorticity perturbations. The linearisation of potential vorticity may not be legitimate. Nonlinear features of the potential vorticity may suppress the relationships suggested above. Thus an important question which this study wishes to examine is whether this analysis transfers to the full non-linear potential vorticity transformation on the sphere.

hapter 4

hange in control variables: Theoretical Aspects

4.1 Introduction

As mentioned in Chapter1, data assimilation brings together observations and information from a forecast model in some consistent manner. The current means of achieving this at the UK Met. Office involves a formulation of the problem called incremental 3D Variational Data Assimilation (3DVAR). In this chapter we wish to make precise the description of a change of 'control variables' for this formulation of the data assimilation problem. T control variables in relation to what an 'idealised' set of control variables should be like.

In Section 4.5, we discuss the advantages and disadvantages of choosing potential vorticity as the balanced control variable with the departure from linear balance and divergence as the two other unbalanced variables. We describe a method to evaluate control variables with a description of the boundary conditions needed. The method readily presents five variables of which three are needed as control variables. We discuss the various choices for the three variables.

In Section 4.6, using the ideas in McIntyre and Norton's paper on balanced models that conserve potential vorticity [36], we can evaluate a higher order approximation to the balanced part of the flow at a given time. From this higher order approximation we can find an estimate of the balanced parts of the unbalanced variables. We adapt this theory and propose a method to evaluate balanced corrections for various sets of control variables, identifying the associated divergence tendency of each set. This allows a comparision to be made in Chapter 7 between the present set of control variables and the new potential vorticity-based set.

As shown in Section 3.9, the height and wind fields behave differently under various Burger regimes. This is also true with control variables. In Section 4.7 we identify how the potential vorticity control transform behaves under various regimes and show that the solution given by the current control variable set and the new control variable sets are the same in high Burger regimes and vary in low Burger regimes.

4. Data Assimilation

The majority of linear data assimilation methods can be considered in terms of a prototype data assimilation problem, using least squares estimation. We specify this problem by showing how it relates to the 3DVAR formulation. We then present incremental 3DVAR as a tec the covariances B and O are too large to calculate explicitly and data assimilation methods are needed to curtail this difficulty. The Optimal Interpolation method assumes that only a few observations are important in calculating each analysis increment, and so only considers observations in local proximity to model variables. A typical variational method avoids the calculation of K. This is written as:

Minimise $\mathcal{J}$ with respect to $\boldsymbol{x}$, where

$$\begin{aligned} \mathcal{J} &= (\boldsymbol{x} - \boldsymbol{x}_b)^T B^{-1} (\boldsymbol{x} - \boldsymbol{x}_b) + (\boldsymbol{y} - H\boldsymbol{x})^T O^{-1} (\boldsymbol{y} - H\boldsymbol{x}), \qquad (4.4) \\ &= \mathcal{J}_b(\boldsymbol{x}) + \mathcal{J}_o(\boldsymbol{x}). \end{aligned}$$

the UK Met. Office, applies a low resolution correction to a high resolution background. The low resolution incremental problem is a inner loop of the minimisation procedure and is solved for each update of the full high resolution problem [32]. The method is described by minimising the objective functional $J(\boldsymbol{w})$, where

$$\mathcal{J}(\boldsymbol{w}) = \boldsymbol{w}^T B^{-1} \boldsymbol{w} + (\boldsymbol{d} - \mathbf{H}\boldsymbol{w})^T O^{-1} (\boldsymbol{d} - \mathbf{H}\boldsymbol{w}) \tag{4.6}$$

and

- the variable increment is $\boldsymbol{w} = \boldsymbol{x} - \boldsymbol{x}_b$,
- $\boldsymbol{d} = \boldsymbol{y} - H(\boldsymbol{x}_b)$ are the observation increments. $\boldsymbol{y}$ are the full observation values. The nonlinear function H is being used to interpolate the background field to the position of the data points. The linearisation of $H(\boldsymbol{x})$ gives $H(\boldsymbol{x}) = H(\boldsymbol{x}_b) + \mathbf{H}\boldsymbol{w}$.

The variables in which the objective function (4.6) is minimised are called control variables. The cTD!‘Tiables.

this control transform a new objective function is minimised:

$$\mathcal{J}(\boldsymbol{\tau}) = \boldsymbol{\tau}^T B_\tau^{-1}\boldsymbol{\tau} + (\boldsymbol{d} - \mathbf{H}(U\boldsymbol{\tau}))^T O_\tau^{-1}(\boldsymbol{d} - \mathbf{H}(U\boldsymbol{\tau})). \tag{4.7}$$

with $\boldsymbol{d} = \boldsymbol{y} - H(\boldsymbol{x}_b)$ and $B_\tau^{-1} = U^T BU$.

The error covariance matrices, $B,,x$ $B_\tau^{:}\ \theta$

different time-scales, shows that the balanced and unbalanced parts of the flow are uncorrelated with one another. We attempt to find a set of control variables which distinguishes between balanced and unbalanced parts more efficiently. In order to do this we establish in the next section a general framework for describing changes between sets of control variables.

4.4 A General Framework to Examine the Change in Control Variables

Consider the transform T as a series of matrix operations $T_1, T_2, \cdots T_m$, which when applied to the original variables stored in a vector $\boldsymbol{x}^0$ of size $n \times 1$, produces a vector $\boldsymbol{y}^0$ of size $n \times 1$ which contains the control variables. This is given by

$$\boldsymbol{y}^0 = T_m \cdots T_2 T_1 \boldsymbol{x}^0. \tag{4.8}$$

We denote the reverse transformation U by a series of operations $U_1, U_2, \cdots U_m$ from $\boldsymbol{y}^0$ to $\boldsymbol{x}^0$, with

$$\boldsymbol{x}^0 = U_m \cdots U_2 U_1 \boldsymbol{y}^0. \tag{4.9}$$

Unlike the full transforms U and T, the matrix operations need not be non-singular and are allowed to project or restrict the variables concerned.

We can consider each operation in turn setting

$$\begin{aligned} \boldsymbol{x}^i &= T_i \boldsymbol{x}^{i-1}, \\ \boldsymbol{y}^i &= U_i \boldsymbol{y}^{i-1}, \qquad \text{for} \quad i = 1, \cdots, m, \end{aligned} \tag{4.10}$$

with

$$\boldsymbol{y}^0 = \boldsymbol{x}^m,$$

$$\boldsymbol{x}^0 = \boldsymbol{y}^m. \tag{4.11}$$

Thus we can relate any $\boldsymbol{x}^i$ with any vector $\boldsymbol{y}^j$ by

$$\boldsymbol{x}^i = \left(\prod_{l=1}^{l=i} T_l \quad \left(\prod_{k=j+1}^{k=m} U_k\right) \boldsymbol{y}^j,\right. \tag{4.12}$$

for $i = 1, \cdots, m$ and $j = 0, \cdots, m-1$.

In particular

$$\boldsymbol{x}^1 = T_1 \boldsymbol{x}^0 = T_1 U_m \boldsymbol{y}^{m-1}. \tag{4.13}$$

and if $\boldsymbol{x}^1 = \boldsymbol{y}^{m-1}, \forall \boldsymbol{y}^{m-1}$, then T_1 is the inverse of U_m.

We now formalise our definitions T_1, U_m in a way similar to a treatment of control variables given by unpublished work of Tim Payne [42]. His description is in terms of general infinite dimensional operators. We present the change between control variables as a finite dimensional problem. Thus the linear differential operators presented in the control variable transforms in Sections 4.4.1, 4.5, 4.7, are finite dimensional approximations to the true analytic differential operators.

Let us denote the model variable increments as

$$\boldsymbol{x}^0 = \begin{pmatrix} u' \\ v' \\ h' \end{pmatrix}, \tag{4.14}$$

with the new set of control variables denoted as

$$\boldsymbol{x}^1 = \boldsymbol{y}^{m-1} = \begin{pmatrix} y_1' \\ y_2' \\ y_3' \end{pmatrix}. \tag{4.15}$$

Each of the model variables, u', v', h', and control variables y_1', y_2', y_3' are considered to be discrete and represented by vectors of size $s \times 1$.

We set three projections from the control v

denoted by h_{base}, $\mathbf{u}_{base}$. We subtract the same linearisation state from both sets of full fields to give the respective perturbed fields $\mathbf{u}_p^*$, h_p^*, $\mathbf{u}_{base}^*$, h_{base}^* where

$$\begin{aligned}
\mathbf{u}_p^* &= \mathbf{u} - \overline{\mathbf{u}}, \\
h_p^* &= h - \overline{h}, \\
\mathbf{u}_{base}^* &= \mathbf{u} - \overline{\mathbf{u}}, \\
h_{base}^* &= h_{base} - \overline{h}_{base}.
\end{aligned} \tag{4.20}$$

The height and wind increments are defined by the difference between base height and wind perturbations h_{base}^*, $\mathbf{u}_{base}^*$, and the full height and wind perturbations h_p, $\mathbf{u}_p$. They are given by

$$\begin{aligned}
\mathbf{u}' &= \mathbf{u}_p^* - \mathbf{u}_{base}^*, \\
h' &= h_p^* - h_{base}^*.
\end{aligned} \tag{4.21}$$

The properties of these linearisation states is given in Section 2.4 while the means in which they are calcluated is left to Section 5.3.2.

The change in control variables transforms the height and wind increments into the streamfunction ψ', velocity potential χ' and unbalanced height h'_{ub}. The full streamfunction increment is considered balanced. The unbalanced height is the difference between the full height increment and the balanced height increment, obtained from the streamfunction using the linear balance equation.

We set $\mathbf{u}' = u'\mathbf{i} + v'\mathbf{j}$ with $\mathbf{i}, \mathbf{j}$ being orthonormal vectors on the surface of the sphere and $\mathbf{k}$ being a unit vector pointing radially away from the centre of the sphere. We write

$$T_1^1: \quad \psi' = \nabla^{-2}\left(\mathbf{k} \cdot \nabla \times \mathbf{u}'\right), \tag{4.22}$$

$$T_1^2: \; h'_{ub} \;\; = \;\; h' - \frac{1}{g}\nabla^{-2}\nabla \cdot f\nabla\psi'$$

evaluation of the balanced height h_1' is dependent purely on the rotational part of the flow with the unbalanced height h_2' holding the rest of the height. Thus h_3' is zero; we assume that the velocity potential increment does not contribute to the unbalanced height.

The choice of control variables which are constrained by ψ are not unique; we could be perverse and choose $y_1 = h_b$, by calculating the streamfunction and then applying the linear balance equation. Thus,

$$T_1^1 : \quad h_b' \quad = \quad \frac{1}{g}\nabla^{-2}\nabla \cdot f\nabla\nabla^{-2}\left(\mathbf{k}\cdot\nabla\times\mathbf{u}'\right) \tag{4.26}$$

and

$$U_m^1 : \quad (\mathbf{u}_1', h_1) \quad = \quad \left(\mathbf{k}\times\nabla\left(\left(\nabla\cdot f\nabla\right)^{-1}\nabla^2 g\ h_b\right), h_b\right), \tag{4.27}$$

with the other variables and operators the same as before.

There are two reasons why this is not used. In data assimilation the U transform is applied every time during the minimisation procedure. The procedure to calculate the winds from the balanced height is computationally more costly taking more cpu time to evaluate. Also, as noted in Section 3.5, it is noticeably less accurate compared to using just the streamfunction because we need to use the reverse linear balance equation.

There are additional issues to consider when using LBE in a data assimilation context. The dynamical behaviour of the winds in the tropics is not captured by the LBE. Thus observations in the tropics are going to be inconsistent with the dynamical behaviour of LBE. The observations for the winds are also comprehensive on horizontal surfaces, while their vertical structure is less well known. Meanwhile,

need an additional balance constraint. We choose this to be the LBE. This potential vorticity inversion is a somewhat cruder version of McIntyre and Norton's [36] first-order direct inversion, which uses a Charney balance condition instead of the LBE. The LBE is used in the inversion, because this allows a direct comparison to be made between using the rotational wind to define the balance and using potential vorticity. We do this by solving the equations representing the linear balance and linear potential vorticity increments simultaneously for ψ_b and h_b, as

$$\nabla \cdot f\nabla\psi_b - g\nabla^2 h_b = 0, \tag{4.28}$$

$$\nabla^2\psi_b - \overline{q}h_b = \mathbf{k}\cdot(\nabla\times\mathbf{u}') - \overline{q}h'. \tag{4.29}$$

The height increment and wind increments and the potential vorticity linearisation state are known before application of this potential vorticity inversion. The height and winds increments, h', $\mathbf{u}'$, are defined in equation (4.21) and the potential vorticity linearisation state $\overline{q}$ is given by (2.63).

From this coupled system we obtain a 'balanced' height h_b and a 'balanced' wind, defined by $u_b = \mathbf{k}\times\nabla\psi_b$. The 'balanced' wind increment is non-divergent, and approximates the full rotational wind increment for high Burger number regimes. The rest of the rotational wind is described as having no potential vorticity increment and conserving a departure from linear balance. This can be obtained in one of two ways, either by subtracting the balanced wind and height from the full rotational wind and height, or by explicitly solving the simultaneous system

$$\nabla \cdot f\nabla\psi_{ub} - g\nabla^2 h_{ub} = \nabla\cdot f\nabla\psi' - \nabla^2 h' \tag{4.30}$$

$$\nabla^2\psi_{ub} - \overline{q}h_{ub} = 0, \tag{4.31}$$

where the unbalanced rotational wind is defined to be $u_{rub} = \mathbf{k}\times\nabla\psi_{ub}$ and the unbalanced height is denoted by h_{ub}. The equivalence of the two methods to calculate the unbalanced height and unbalanced rotational wind is readily seen by adding equation (4.28) to (4.30) and (4.29) to (4.31), to give

$$\nabla \cdot f\nabla\left(\psi_b + \psi_{ub}\right) - g\nabla^2\left(h_b + h_{ub}\right) = \nabla \cdot f\nabla\psi' - \nabla^2 h' \tag{4.32}$$

$$\nabla^2\left(\psi_b + \psi_{ub}\right) - \overline{q}\left(h_b + h_{ub}\right) = \mathbf{k} \cdot \left(\nabla \times \mathbf{u}'\right) - \overline{q}h', \tag{4.33}$$

The third variable contains the remaining information, namely the divergent part of the wind and is stored in the velocity potential.

The above description produces five different variables, ψ_b', ψ_{ub}', χ', h_b', h_{ub}', which together give the original height and wind fields. From these five variables we choose three control variables, from which the ignored part of the height and wind fields is easily recovered. To mimic the dynamic behaviour of the shallow water equations we choose the control variables so that one is balanced and two others are unbalanced.

There are four possible choices to obtain such a control set. Each method we now discuss.

4.5.1 Method 1: ψ_b', ψ_{ub}', χ'

$$T_1^1: \quad \psi_b' = \Big[\nabla \cdot f\nabla -$$

and substituting $g\nabla^2 h_b$ from (4.28) with $\nabla \cdot f\nabla\psi_b$. Likewise T_1^2 is given by substituting into (4.30) $\frac{1}{q}\nabla^2\psi$

A difficulty lies in the calculation of the balanced height. Within equations (4.28), (4.29) not only the second order derivatives in ψ_b need to be substituted but also the first order derivatives as well. We present an approach to alleviate this problem. We calculate the balanced streamfunction and then use the linear balance relation to obtain the balanced height.

$$T_1^1 : \quad h_b' = \frac{1}{g}\nabla^{-2}\nabla \cdot f\nabla\psi_b' \tag{4.47}$$

where ψ_b' is given by either (4.34).

Similarly, we may obtain h_{ub} from ψ_{ub}, using the fact that the linearised potential vorticity increment conserved by these two variables is zero, giving

$$h_{ub}' = \frac{1}{q}\nabla^2\psi_{ub}' \tag{4.48}$$

where ψ_{ub}' is given by (4.35).

The associated U_m^1 transformation uses reverse linear balance to derive the balanced part of the rotational wind.

$$U_m^1 : \quad (\mathbf{u}_1'^T, h_1) \quad = \quad (\mathbf{k} \times \nabla\left(\nabla \cdot f\nabla\right)^{-1}\nabla^2 g h_b', h_b')(\mathbf{t}. \; , h_1) \quad = \quad)$$

The two remaining methods are the control variables sets h'_b, ψ'_{ub}, χ' and ψ'_b, h'_{ub}, χ'. The equations relating to these control variables are given above.

In a shallow water context on a doubly periodic f-plane we showed in Section 3.8 that the slow mode relating to the zero eigenvalue is in geostrophic balance and is described by a linearised potential vorticity increment. The other two variables, the divergence and departure from geostrophic balance, are linear combinations of the unbalanced eigenvalues of the system. On this f-plane the balanced variable is independent from the unbalanced part. Ideally, we would wish the unbalanced components to represent the eigenvalues of the unbalanced part. Unfortunately this in not the case.

In summary, the changes in control variable described in this section do have certain difficulties: namely the problem with the linearisation of the potential vorticity going to zero at the equator and the problem of constraining the control transforms (4.41) by $\mathbf{k} \cdot \nabla \times f \nabla \psi_b = 0$ and (4.42) by $\mathbf{k} \cdot \nabla \times f \nabla \psi_{ub} = 0$. Balanced and unbalanced ψ variables seem better than the corresponding balanced and unbalanced height, due to the need to solve the reverse LBE equation in the corresponding U transform. For these reasons we solve for the balanced variables in their original formulation given in (4.28), (4.29).

4.5.3 Conditions for Solving the Potential Vorticity-based Change in Control Variables

The boundary conditions for solving the simultaneous system (4.28), (4.29) comes from the consideration of the solution of the linear balance equation and the existence and uniqueness conditions, necessary for the solution of a Poisson equation on a sphere. We are considering solutions over the hemisphere. This is done by solving over the sphere and making the right-hand side of (4.29) anti-symmetric about the equator. This enforces ψ_b to be antisymmetric and h_b to be symmetric about the equator. This is equivalent to setting

$$\frac{\partial h_b}{\partial \theta}(0, \lambda$$

tendencies that are small.

Let us first consider control variable increments with linearisation states $\overline{\mathbf{u}} = 0$ and $\overline{h} = H$, where H is constant. If we consider the linearisation of the shallow water equations about such states and introduce only the balanced variables, from whatever method, into the respective divergence equation (2.50), we get a divergence tendency of zero. This is due to the divergence of advective term in the SWEs momentum equation (2.56) being comprised of squared perturbations. If we, however, consider the linearised divergence equation linearised about a time-varying state and apply the balanced variables, the divergence of advective terms of (2.37) remains. The divergence tendency of the balanced control variable is then given by

$$\frac{\partial \delta_r}{\partial t} = -\nabla^2 \left[(\mathbf{v_r}' \cdot \overline{\mathbf{v}}') \right] + \mathbf{k} \cdot \nabla \times \left(\overline{\zeta} \mathbf{v_r}' + \zeta' \overline{v} \right), \quad \text{LB method} \qquad (4.53)$$

$$\frac{\partial \delta_p}{\partial t} = -\nabla^2 \left[(\mathbf{v_{pv}}' \cdot \overline{\mathbf{v}}') \right] + \mathbf{k} \cdot \nabla \times \left(\overline{\zeta} \mathbf{v_{pv}}' + \zeta' \overline{v} \right) \quad \text{PV method} \qquad (4.54)$$

where the LB method is the standard change in control variables described by (4.22) and the PV method is the name we give to the change in control variables based of potential vorticity inversion described by (4.29), (4.28) in Section 4.5, $\mathbf{v_r}$ is the rotational wind and $\mathbf{v_{pv}}$ is the balanced rotational wind deriv by definition sets both the divergence tendency of the nonlinear divergence equation and the second order partial time derivative of the divergence to zero. By using a similar concept we derive in the next subsection a correction to the balanced wind and heights given by the LB and PV methods which sets the divergence tendency of the divergence equation linearised about a time-varying state to be zero. This method has the added benefit that the correction identifies balanced parts in unbalanced variables.

4.6.1 Approximation of Divergence Tendencies of Balanced Corrections to Unbalanced Variables

In the direct second-order potential vorticity inversion model in McIntyre and Norton's paper [36], one of the equations which close their dynamical system enforces the second partial time derivative of the divergence to be set to zero. We derive a similar equation which uses a balanced correction to find the divergent wind. This is done by first applying the local partial time operator to the divergence equation (2.61) linearised about time-varying linearisation states $\overline{h}, \overline{\mathbf{v}}, \overline{\zeta}$ as defined in Section 2.4, giving

$$\begin{aligned} \frac{\partial^2 \delta'}{\partial^2 t} - \mathbf{k} \cdot \nabla \times \left(\left(\overline{\zeta} + f \right) \frac{\partial \mathbf{v}'}{\partial t} + \frac{\partial \left(\overline{\zeta} + f \right)}{\partial t} \mathbf{v}' + \frac{\partial \zeta'}{\partial t} \overline{\mathbf{v}} + \zeta' \frac{\partial \overline{\mathbf{v}}}{\partial t} \right) & \\ + \nabla^2 \left(g \frac{\partial h'}{\partial t} + \frac{\partial \mathbf{v}'}{\partial t} \cdot \overline{\mathbf{v}} + \frac{\partial \overline{\mathbf{v}}}{\partial t} \cdot \mathbf{v}' \right. &= 0, \quad (4.55) \end{aligned}$$

where

$$\frac{\partial \mathbf{v}'}{\partial t} = -\nabla \left(\overline{\mathbf{v}} \cdot \mathbf{v}' \right) - \left(\overline{\zeta} + f \right) \mathbf{k} \times \mathbf{v}' - \zeta' \mathbf{k} \times \overline{\mathbf{v}} - g \nabla h', \quad (4.56)$$

$$\frac{\partial \zeta'}{\partial t} = -\nabla \cdot \left(\left(\overline{\zeta} + f \right) \mathbf{v}' + \zeta' \overline{\mathbf{v}} \right), \quad (4.57)$$

$$\frac{\partial h'}{\partial t} = -\overline{\mathbf{v}} \cdot \nabla h' - \mathbf{v}' \cdot \nabla \overline{h} - h' \nabla \cdot \overline{\mathbf{v}} - \overline{h} \nabla \cdot \mathbf{v}'. \quad (4.58)$$

$$\frac{\partial \overline{\mathbf{v}}}{\partial t} = -\nabla \left(\frac{\overline{\mathbf{v}} \cdot \overline{\mathbf{v}}}{2} \right) - \left(\overline{\zeta} + f \right) \mathbf{k} \times \overline{\mathbf{v}} - g \nabla \overline{h}, \quad (4.59)$$

$$\frac{\partial \overline{\zeta}}{\partial t} = -\nabla \cdot \left(\left(\overline{\zeta} + f \right) \overline{\mathbf{v}} \right), \quad (4.60)$$

$$\frac{\partial \overline{h}}{\partial t} = -\overline{\mathbf{v}} \cdot \nabla \overline{h} - \overline{h} \nabla \cdot \overline{\mathbf{v}}. \quad (4.61)$$

Incorporating (4.56) - (4.61) into (4.55) and setting the second partial time derivative of the divergence to zero leaves on simplifying

$$\mathbf{k} \cdot \nabla \times \left(\left(\overline{\zeta} + f \right) \left(\nabla \left(\overline{\mathbf{v}} \cdot \mathbf{v}' \right) \right) \right) + \left(\overline{\zeta} + f \right)^2 \nabla \cdot \mathbf{v}' + \nabla \left(\overline{\zeta} + f \right)^2 \cdot \mathbf{v}'$$

$$+\mathbf{k} \cdot \nabla \times \left[\left(\overline{\zeta} + f \right) \left(\zeta' \mathbf{k} \times \overline{\mathbf{v}} \right) \right] + g \mathbf{k} \cdot \nabla \times \left[\left(\overline{} \right. \right.$$

increments involving divergence and are rewritten as $\left(\overline{\zeta}+f\right)^2\delta'$, $g\nabla^2\left(\overline{h}\delta'\right)$. We wish to make the divergence increment the variable to be solved for, so we keep those two terms on the left and place the rest on the right hand side.

This gives a modified Helmholtz equation to be solved of the form

$$\nabla^2\left(g\overline{h}\delta_b\right) - \kappa\left(g\overline{h}\delta_b\right) = \varpi \tag{4.63}$$

where κ is given by

$$\kappa = \frac{(\zeta+f)^2}{g\overline{h}} \tag{4.64}$$

and ϖ

Table 4.1: The scaling of various terms in equation (4.62) ,with the characteristic length scales $L \approx 10^3 m$, the characteristic height linearisation state $\overline{H} \approx 10^3 m$, the characteristic velocity linearisation state $\overline{U} \approx 10^1 ms^{-1}$, the height increments $H \approx 10^2 m$, the wind increments $U \approx 10^1 ms^{-1}$, $f \approx 10^{-4} s^{-1}$ and $g \approx 10$

Terms considered	Dimensional scaling	Size of term
$\left(\overline{\zeta}+f\right)^2 \nabla \cdot \mathbf{v}'$, $\nabla \left(\overline{\zeta}+f\right)^2 \cdot \mathbf{v}'$	$\frac{f^2 U}{L}$	10^{-13}
$g\nabla^2 \left(\mathbf{v}' \cdot \nabla \overline{h}\right)$, $g\nabla^2 \left(\overline{h} \nabla \cdot \mathbf{v}'\right)$	$\frac{g\overline{H}U}{L^3}$	10^{-13}
$\mathbf{k} \cdot \nabla \times \left[\left(\overline{\zeta}+f\right)\left(g\nabla h'\right)\right]$	$gfH,$	

part of the flow lies in the departure from linear balance. Suppose we consider the divergence equation, linearised about a time-varying linearisation state (2.61). We presume that the total balanced parts of the flow satisfies this equation and has a divergence tendency of zero.

Since we are considering a linearisation of the divergence equation, it is possible to separate the balanced part of the divergence equation that we know, from those parts that we do not. Thus the balanced contribution to the divergence equation is given by

$$-\mathbf{k}\cdot\nabla\times\left(\left(\overline{\zeta}+f\right)\mathbf{v_1}+\zeta_1\overline{\mathbf{v}}\right)+\nabla^2\left(gh_1+\mathbf{v_1}\cdot\overline{\mathbf{v}}\right) = \mathbf{k}\cdot\nabla\times\left(\left(\overline{\zeta}+f\right)\mathbf{v_2}+\zeta_2\overline{\mathbf{v}}\right) -\nabla^2\left(gh_2+\mathbf{v_2}\cdot\overline{\mathbf{v}}\right) \qquad (4.66)$$

where $\mathbf{v_1}$, $\mathbf{h_1}$ is the balanced velocity and height contribution the variable describing a departure from linear balance. The wind $\mathbf{v_2}$ is defined as

$$\mathbf{v_2} = \mathbf{v_{pv}} + \mathbf{v_{bd}}, \qquad h_2 = h_{pv} \qquad (4.67)$$

or

$$\mathbf{v_2} = \mathbf{v_{lb}} + \mathbf{v_{bd}}, \qquad h_2 = h_{lb}, \qquad (4.68)$$

where $\mathbf{v_{bd}}$ is the balanced divergent ‘ ‘ T D ! Ψ e r g e n ” T j ! ‘ ‘ T o j ! ‘ ‘ n ! Ψ ” n g T h in the kernel of the linearised potential vorticity increment, as we assumed in the control variables that unbalanced flow contained no linearised potential vorticity.

benefit of increased accuracy in the balanced variable. For this reason the above procedure is used only for comparisons between the PV and LB methods.

4.7 Control Variables and Burger Regimes

The PV method approximates the LB method under high Burger regimes since the majority of the linearised potential vorticity is held in the rotational wind in such regimes. For very small Burger number regimes for which the linearised potential vorticity is predominantly composed of a weighted height increment, $\overline{q}h'$, the PV method approximates the control variables set in which the height increment is considered to be the balanced variable. This is written as

$$\begin{aligned} T_1^1: \quad h' &= h', \\ T_1^2: \quad \psi'_{ub} &= \nabla^{-2}\left(\mathbf{k}\cdot(\nabla\times\mathbf{u}')\right) - \left(\nabla\cdot(f\nabla)\right)^{-1}\nabla^2 gh', \\ T_1^3: \quad \chi' &= \nabla^{-2}\left(\nabla\cdot\mathbf{u}'\right). \end{aligned} \tag{4.73}$$

The inverse transform U_m is

$$\begin{aligned} U_m^1: \quad (\mathbf{u}_1'^T, h_1) &= \left(\left(\nabla\cdot(f\nabla)\right)^{-1}\nabla^2 gh', h'\right) \\ U_m^2: \quad (\mathbf{u}_2'^T, h_2) &= (\mathbf{k}\times\nabla\psi_{ub}, 0) \\ U_m^3: \quad (\mathbf{u}_3'^T, h_3) &= (\nabla\chi', 0) \end{aligned} \tag{4.74}$$

The above change in control variables involves solving the reverse LBE which we have already mentioned as being problematic. Though the PV method is approximating this change in control variables, it may not have the same problems around the equator. This is because around the equator, due to $f \rightarrow 0$, the Burger number gets increasingly large and the PV method is going to approximate the LB method in these regions.

We need to examine the performance of LB and PV methods for a wide range of Burger numbers. Though it seems that there should be better results using the PV method, compared to the LB method for low Burger number, it is unclear as to the cutoff value in the Burger number when these improvements are noticable. The cutoff value should be close to 1, but this is to be checked in the experiments in Chapter 7.

4.8 Conclusion

In this chapter we have defined a change in control variables in terms of the data assimilation problem. A framework is proposed in which control variables can be examined. It is used to view the current change in control variables at the UK Met. Office when applied to SWEs on a sphere. A change in control variables is defined which conserves a potential vorticity increment. The dynamical properties of an ideal set of control variables are discussed. We then consider the relationship between control variables and divergence tendency and present a means to establish the respective performance, by finding a way to evaluate the divergence tendency in the unbalanced variables. The chapter concludes with an examination of how the control variables from the PV method vary in behaviour with Burger number.

hapter 5

Numerical ackground

5.1 Introduction

In this chapter we present the numerical details of the algorithms used in Chapter 7. The first part of this chapter relates to the shallow water equations. Section 5.2 gives some of the numerical details of the UK Met. Office's shallow water equation model on a sphere. In Section 5.3 we describe two different initial conditions: one described by the Rossby-Haurwitz wave on the sphere (3.34) - (3.36) and the other representing a realistic atmospheric situation.

Throughout Chapters 2, 4 we use linearisation states $\overline{h}$, $\overline{\mathbf{u}}$, $\overline{q}$. In Section 5.4 the experimental details of various types of linearisation states are presented that are used in the experiments in Chapter 7. The third part of this chapter considers the Poisson equation. Understanding the numerical properties of the Poisson equation not only gives the tools to solve the linear balance equation (LBE) and obtain the streamfunction and velocity potential from the vorticity and divergence - it also presents a method of solution which we use later in Chapter 6 to solve a control

Figure 5.1: Arakawa C grid

$$\begin{array}{ccc} h_{i,j} & u_{i,j} & h_{i,j+1} \\ \\ v_{i,j} & & v_{i,j+1} \\ \\ h_{i+1,j} & u_{i+1,j} & h_{i+1,j+1} \end{array}$$

variable transform based on conserving potential vorticity (4.29). The numerical evaluation of the Poisson equation is discussed in Section 5.5 while in Section 5.5.1 we consider the question of existence and uniqueness of solutions to this problem.

In the last two Sections, various finite difference approximations are presented, for which we give validatory evidence of their correct evaluation.

5. Shallow ater Equations: General Experimental Details

The numerical model approximating the shallow water equations calculates the height and wind fields on a staggered mesh called an Arakawa C grid. The relative positions of h, u, v are given in Figure 5.1.

The code which solves the SWEs is that used within the UK's Met. Office numerical weather prediction model (Unified Model). It is a semi-Lagrangian, semi-implicit, predictor-corrector scheme. The wind field is predicted for the next time step and the difference between the present time step and the next is calculated and

Provided we consider a high Burger regime, the unbalanced parts remain small compared to the balanced parts.

Since Philips [44], investigators have been using this wave to provide initial conditions for the SWEs. Throughout this thesis we choose the wavenumber to be equal to 4, as we want the field to be stable. Following Hoskins [27], Rossby-Haurwitz waves with zonal wavenumbers less than or equal to 5 are commonly considered to be stable while those greater than 5 are considered unstable. Recently in papers [3], [56], the stability of the Rossby-Haurwitz wave for zonal wavenumber $R = 4$ has been put into question, due to significant differences between between various 5-day model simulations using different numerical models. Also certain numerical models provide solutions which disrupt both the basic symmetry of the U, H fields about the equator and also the antisymmetry of the V field. The numerical techniques we use to evaluate the change in control variables rely on these symmetries. Fortunately, the Met Office Semi-Lagrangian SWE model which we use preserves the symmetries needed.

5.3.2 Real initial conditions

Case 7c was used originally by Baumhefner and Bettge 4.r

$VDG7.11.cdf$ found in $f\ p : //f\ p.cgd.ucar.edu/pub/je\ /shallow/nmini\ /$ with mean depth 10.

$$\overline{h}(\theta) = h_l \tag{5.7}$$

$$\overline{v} = 0. \tag{5.8}$$

Since $\overline{h}q^* \approx \nabla^2\psi^* - \overline{q}h^*$ to order $O((h^*)^2, h^*\nabla^2\psi^*)$, the linearised potential vorticity perturbation is only accurate provided $\overline{h}q^* >> O(\overline{q}(h^*)^2/\overline{h}, h^*\nabla^2\psi^*)$. When $\overline{h}$ is small, as for low Burger regimes, there is a greater opportunity for this criterion to be violated, especially when q^*, h^* and ψ^* involve relatively large departures from respective linearisation states. This is why a latitudinally-varying linearisation state is considered, as the departures from the linearisation states are going to be much smaller compared to when $\overline{u} = 0$, $\overline{v} = 0$ and $\overline{h} = H$.

The effect of choosing latitudinally varying states that satisfy the PV method gives linearisation states that are in geostrophic balance. A linearisation state that satisfies a balance condition is necessary in Section 4.6 to identify correctly the divergence tendency in the unbalanced variables.

5.5 Poisson Equation

The Poisson equation on the sphere is given by

$$\frac{1}{a^2\cos^2\theta}\frac{\partial^2\phi}{\partial\lambda^2} + \frac{1}{a^2\cos\theta}\frac{\partial}{\partial\theta}\left[\cos\theta\frac{\partial\phi}{\partial\theta}\right] = F(\lambda,\theta), \tag{5.9}$$

where a is the radius of the sphere, λ and θ are the longitude and latitude, ϕ is the solution and F is a known forcing term.

The solution of the Poisson equation over a sphere is required for the calculation of the streamfunction, velocity potential and the calculation of balanced height from the streamfunction using the Linear Balance equation. The first step to solving the Poisson equation is to apply discrete fast Fourier transforms (DFFTs) in the longitudinal direction. This provides second order ordinary differential equations (ODEs) for each zonal wavenumber. These ODEs are discretised using a finite volume approach that is equivalent to a 2^{nd} order centered finite difference method. They are solved by applying a standard tri-diagonal solver. The solution to the Poisson equation is obtained by applying an inverse fast Fourier transform at every value of latitude considered. As the method of solution is similar to that given by Moorthi [38] we present only the key implementational details and leave the definition of the DFFT and its inverse to that paper.

Consider a regular latitude/longitude grid over a sphere, with the grid spacing in the latitude and longitude denoted respectively by

$$\Delta\theta = \frac{\pi}{N-1} \qquad \text{and} \qquad \Delta\lambda = \frac{2\pi}{\ }, \tag{5.10}$$

where N is the number of points in the co-latitudinal direction, indexed as i, going from the north pole to the south pole. Similarly, is the number of grid points in the longitudinal direction. The longitudinal dimension to the grid points, denoted by index j, are numbered positively in an anti-clockwise direction around the north pole. We stipulate that $= 2^n 3^n$ where m, n are integers. This choice makes the Fourier transform and its inverse efficient to use. We also set N to be odd. This allows grid values with index $i = \frac{N+1}{2}$ to lie on the zero latitude.

We are solving the discrete problem on a sphere where $\theta \in [-\frac{\pi}{2}, \frac{\pi}{2}]$, $\lambda \in [0, 2\pi]$ and θ, λ are the latitude and the longitude. Periodic boundary conditions are assumed for the longitude. The problem is scaled onto the surface iNe a sphere of problem is known, the rescaling back onto a spherical Earth is performed. Thus, for the following discussion, we consider the Poisson equation on a sphere of unit radius.

Application of the DFFT gives a tridiagonal system to be solved for each wavenumber considered. For $i = 2, \cdots, N-1$ and generic wavenumber k, the tridiagonal system takes the form

$$\begin{aligned} -\frac{k^2\pi^2\tilde{\phi}_i}{\cos(\theta_i)} + & \\ \frac{\cos(\theta_{i-1/2})(\tilde{\phi}_{i-1} - \tilde{\phi}_i) + cos(\theta_{i+1/2})(\tilde{\phi}_{i+1} - \tilde{\phi}_i)}{\Delta\theta^2} &= \cos(\theta_i)\tilde{f}_i, \end{aligned} \tag{5.11}$$

where $\tilde{\phi}_i$, $\tilde{f}_i$ are the complex coefficients of the solution and right-hand side for latitude circle i. The grid and half grid values of the latitude are defined as:

$$\begin{aligned} \theta_i &= \frac{\pi}{2} - (i-1)\Delta\theta, & \text{for } i = 1, \cdots, N, \\ \theta_{i+1/2} &= \frac{\pi}{2} - (i - \frac{1}{2})\Delta\theta, & \text{for } i = 1, \cdots, N-1, \end{aligned} \tag{5.12}$$

To complete the description of the tridiagonal system, we need equations for the polar values. The equation at each pole is derived using the integral, finite volume approach as presented by Barros [2]. The equation is derived as follows:

$$\begin{aligned} \int_0^{2\pi} \int_{\frac{\pi}{2}-\frac{\Delta\theta}{2}}^{\frac{\pi}{2}} \nabla^2\phi \cos\theta d\theta d\lambda &= \sum_{l=1}^{M} \int_{(l-1)\Delta\lambda}^{l\Delta\lambda} \int_{\frac{\pi}{2}-\frac{\Delta\theta}{2}}^{\frac{\pi}{2}} \nabla^2\phi \cos\theta d\theta d\lambda \\ &= \sum_{l=1}^{M} \int_{(l-1)\Delta\lambda)}^{l\Delta\lambda} -\nabla\phi \end{aligned}$$

(5.13) where F is the scaled right-hand side value at the north pole P_N with the associated surface area V_N. The surface area V_N is the surface area of the spherical cap above latitude $\theta = (\pi - \Delta\theta)/2$.

We observe that in (5.13), a longitudinal mean is taken for both the grid points at the north pole and for $i = 2$. Since $\tilde{\phi}_1$ and $\tilde{\phi}_2$ represent longitudinal means when $k = 0$, equation (5.13) can be rewritten as

$$-\frac{4}{\Delta\theta^2}\tilde{\phi}_1 + \frac{4}{\Delta\theta^2}\tilde{\phi}_2 = \tilde{f}(0)_1. \tag{5.14}$$

For non-zero values of k we stipulate Dirichlet boundary conditions $\widetilde{\phi}_1 = 0$, $\widetilde{\phi}_N = 0$ and solve over the whole sphere. These boundary conditions enforce single values at the poles and give tridiagonal systems of full rank.

When $k = 0$ additional conditions are needed for a unique solution. We consider the problem when the right hand side is either symmetric or anti-symmetric about the equator. When the right hand side is anti-symmetric about the equator there is no difficulty in obtaining a solution. We solve over the upper hemisphere setting a zero Dirichlet boundary condition at the equator. The solution is copied onto the other hemisphere and a sign change is applied.

When $k = 0$ and the right hand side is symmetric about the equator a uniqueness condition needs to be satisfied. Such a problem occurs in this thesis where V_i is given by

$$\begin{aligned}
V_1 &= 2\pi a^2 \frac{\Delta\theta}{2} \cos\theta_{\frac{1}{2}}, \\
V_i &= 4\pi a^2 \Delta\theta \cos\theta_i \qquad\qquad \text{for} \quad i = 2, \ldots, \frac{N-1}{2}. \\
V_{\frac{N+1}{2}} &= 2\pi a^2 \Delta\theta \qquad\qquad (5.17)
\end{aligned}$$

The solution to the tri-diagonal sytem is then copied to the other hemisphere before IDFFT's are used to get the solution to the Poisson equation.

A few additional notes have to be made. The computational procedure for the numerical solution of the Poisson equation is written in the Matlab language. It uses subroutines from the FFTW library [19],[20] that are well known and reliable. The right hand side of the Poisson equation has to satisfy the compatibilit

If w

$f_{i-\frac{1}{}}$

$$\chi = a^2\omega\cos^2\theta + a^2K\cos^R\theta\cos R\lambda \tag{5.33}$$

and the vorticity and streamfunction are given by

$$\zeta = 2\omega\sin\theta - K\sin\theta\cos^R\theta\left(R^2+3R+2\right)\cos R\lambda, \tag{5.34}$$

$$\begin{aligned}\delta &= -2\omega\left(\cos^2\theta - 2\sin^2\theta\right)\\ &\quad +K\cos^{R-2}\theta\left(-R^2 - R\cos^2\theta + R^2\sin^2\theta\right)\cos R\lambda.\end{aligned} \tag{5.35}$$

The right hand side of LBE is

$$\begin{aligned}\nabla\cdot f\nabla\psi &= -2\Omega R^2K\cos^{R-2}\theta\sin^2\theta\cos R\lambda\\ &\quad +2\Omega\left[2\omega\sin^2\theta - \omega\cos^2\theta\right.\\ &\quad +K\cos R\lambda\left(R^2\cos^{R-2}\theta\sin^4\theta - (4R+2)\cos^R\theta\sin^2\theta\right.\\ &\quad \left.\left.+\cos^{R+2}\theta\right)\right].\end{aligned} \tag{5.36}$$

We use a normalised L_2 vector norm to get estimates of the error between the numerical approximations and the true analytic solutions. The error estimate ε is of the form

$$\varepsilon = \frac{\left(\sum_{i=1}^{N}\sum_{j=1}^{M}\left(\alpha_{i,j}^t - \alpha_{i,j}^a\right)^2\right)^{\frac{1}{2}}}{\left(\sum_{i=1}^{N}\sum_{j=1}^{M}\left(\alpha_{i,j}^t\right)^2\right)^{\frac{1}{2}}} \tag{5.37}$$

for a generic true field α^t and generic approximation α^a.

The third and fourth columns of Table 5.1 show the L_2 error in ζ, δ between the analytic solutions (5.34), (5.35) and the the numerical approximations (5.26), (5.29) applied to the analytic winds (5.30), (5.31) . The far right column of Table 5.1 shows the L_2 error between analytically defined $\nabla\cdot f\nabla\psi$ given by (5.36) and the numerical approximated value given by the numerical discretisation (5.30) using values defined by (5.33). In all three cases, a doubling of the resolution results in

Table 5.1: L_2 error between numerically and analytically defined ζ, δ and $\nabla \cdot f \nabla \psi$ using equation (5.37)

M	N	L_2 error in ζ	L_2 error in δ	L_2 error in $\nabla \cdot f \nabla \psi$
48	33	0.0494	0.0110	0.0197
96	65	0.0126	0.0027	0.0049
192	129			

where (u_r, u_d) is the rotational part of the wind and (v_r, v_d) is the divergent part.

Second order centered finite difference approximations are used, where the ψ and χ fields coincident with the height positions of the Arakawa C grid, giving wind fields consistent with the considered staggered grid.

$$
\begin{aligned}
u_r(i,j) &= -\frac{1}{a}\frac{\psi_{i-1,j} - \psi_{i+1,j} + \psi_{i-1,j+1} - \psi_{i+1,j+1}}{4\Delta\theta} \\
v_r(i,j) &= \frac{1}{a\ \cos\theta_{i+\frac{1}{2}}}\frac{\psi_{i,j+1} - \psi_{i,j-1} + \psi_{i+1,j+1} - \psi_{i+1,j-1}}{4\Delta\lambda} \\
u_d(i,j) &= \frac{1}{a\ \cos\theta_i}\frac{\chi_{i,j+1} - \chi_{i,j}}{\Delta\lambda} \\
v_d(i,j) &= \frac{1}{a}\frac{\chi_{i,j} - \chi_{i+1,j}}{\Delta\theta}
\end{aligned}
\tag{5.41}
$$

for $i = 1, \ldots, N$ and $j = 1, \ldots,$ with ghost points (i,j) indexed as

$$
(i,0) \;=\; (i,\ \ ), \qquad (i,\ \ +1) = (i,1) \quad \text{for} \quad i = 1,\ldots,N,
$$

due to periodicity in longitudinal direction. In addition, for $i = 1, N$, the stencil of the discretisation goes over the pole such that ghosts point are:

$$
\begin{aligned}
(0,j) &= (1, j + \ \ /2) \ \text{ if } j \leq \ \ /2, \qquad (1, j - \ \ /2) \ \text{ if } j > \ \ /2; \\
(N+1,j) &= (N, j + \ \ /2) \ \text{ if } j \leq \ \ /2, \qquad (N, j - \ \ /2) \ \text{ if } j > \ \ /2;
\end{aligned}
$$

remembering that is chosen to be an even integer. Since the spherical co-ordinate system is degenerate at the poles the values of the u field at such points are set to zero.

Table 5.3 shows the difference in the error between the original and the numerically approximated wind fields using grid-points that do not reside at the pole. The relative error decreases as the resolution is increased consistent with an accuracy

hapter 6

A potential vorticity control variable transform

6.1 Introduction

In Chapter 4, we derive balanced height and balanced rotational wind increments from a potential vorticity increment. We show how these height and wind differences are consistent with the process of geostrophic adjustment. In this chapter we present the n

The assumption that the potential vorticity linearisation state is a function of latitude only is a reasonable assumption when the data is coming from a global shallow water model. Except for around the equator, the major contributor to the absolute vorticity is the Coriolis parameter, which is a function of the latitude only. Also the change in height field at any given latitude seems to vary between 5 % and 20 % of its average value.

This method has a number of advantages. Since the ODE's to be solved for each wavenumber are independent of each other, they can be solved in parallel, making this method quite efficient. Memory requirements are relatively low. Obtaining correct boundary conditions at the poles is well documented in the literature [2]. The equation should be less sensitive to error as we are solving coupled systems of ODEs, instead of a highly sensitive fourth order PDE.

Let us assume that the fields h_b, ψ_b, $\overline{h}q'$ can be described by a discrete inverse fast Fourier transform (DIFFT) in the longitudinal direction, such that

$$\begin{aligned} \mathcal{Q}'(\lambda,\theta) &= \frac{1}{I}\sum_{k=-I/2}^{k=I/2} \tilde{\mathcal{Q}}'^k(\theta)e^{ik\lambda}, \qquad (6.1)\\ h_b(\lambda,\theta) &= \frac{1}{I}\sum_{k=-I/2}^{k=I/2} \tilde{h}^k(\theta)e^{ik\lambda},\\ \psi_b(\lambda,\theta) &= \frac{1}{I}\sum_{k=-I/2}^{k=I/2} \tilde{\psi}^k(\theta)e^{ik\lambda}, \end{aligned}$$

where I is an integer setting a truncation limit to the Fourier approximation, k is the wavenumber, i is equal to $i=\sqrt{-1}$ and

$$\begin{aligned} \mathcal{Q}' &= \overline{h}q' \qquad (6.2)\\ \tilde{\mathcal{Q}}' &= \widetilde{\overline{h}q'} = \mathcal{Q}'^r + i\mathcal{Q}'^i, \end{aligned}$$

$$\begin{aligned}\widetilde{h} &= h^r + ih^i,\\ \widetilde{\psi} &= \psi^r + i\psi^i,\end{aligned}$$

with h^r, h^i, ψ^r, ψ^i, $\mathcal{Q}'^r$, $\mathcal{Q}'^i$ being real. Subsitution of (6.1) into (4.28) and (4.29), produces a coupled system of second order ODE's in θ to be solved for variables $\widetilde{h}$, $\widetilde{\psi}$. The system for a generic value of k is given by

$$-\frac{k^2}{a^2\cos^2\theta}[-g\widetilde{h} + f\widetilde{\psi}] + \frac{1}{a^2\cos\theta}\frac{\partial}{\partial\theta}[-\cos\theta\frac{\partial g\widetilde{h}}{\partial\theta} + f\cos\theta\frac{\partial\widetilde{\psi}}{\partial\theta}] = 0 \tag{6.3}$$

$$-\frac{k^2}{a^2\cos^2\theta}[\widetilde{\psi}] + \frac{1}{a^2\cos\theta}\frac{\partial}{\partial\theta}[\cos\theta\frac{\partial\widetilde{\psi}}{\partial\theta}] - \overline{q}\widetilde{h} = \widetilde{\mathcal{Q}}'. \tag{6.4}$$

To solve this system we obtain $\widetilde{\mathcal{Q}'}$ using a discrete fast Fourier transform (DFFT). Once the system (6.3)-(6.4) is solved, we use DIFFTs to recover the required fields h_b, ψ_b.

To solve (6.4) we need boundary conditions. As with the Poisson equation, the coefficients $\widetilde{h}$ and $\widetilde{\psi}$ are set to zero at the poles for all non-zero wavenumbers in order to enforce single-values at these points.

For $k = 0$ we solve (6.4) over the sphere and enforce a zero value at the equator for the anti-symmetric balanced streamfunction increment. A global uniqueness condition is used of the form,

$$\int_{\theta=-\frac{\pi}{2}}^{\theta=\frac{\pi}{2}} \widetilde{h}(\theta)\cos\theta d\theta = 0. \tag{6.5}$$

The global uniqueness condition applied to $\widetilde{\psi}$,

$$\int_{\theta=-\frac{\pi}{2}}^{\theta=\frac{\pi}{2}} \widetilde{\psi}(\theta)\cos\theta d\theta = 0. \tag{6.6}$$

is automatically satisfied due to the imposed anti-symmetric nature of the right hand side.

the control volume approach is used, both equations are multiplied by the surface area of the segment V_i

where $Q_i = 2\Delta\theta\Omega\mathbf{Q}_i/g$ and $R_i = 2\Omega a^2\Delta\theta\cos\theta_i\tilde{\mathcal{Q}}$

The systems of ODE's for wavenumbers k

which fix the Ψ and $\mathcal{H}$ fields to the addition of a constant. Additional boundary conditions are applied to both Ψ and $\mathcal{H}$. The value of Ψ must be zero at the equator as the balanced streamfunction is anti-symmetric about this value and is assumed to be a continuous smooth function. This additional piece of information is achieved by removing the $\tilde{\Psi}_{\frac{N+1}{2}}$ from the system considered, by extracting the $N+1^{th}$ row and column of the system. A consequence of doing this, is that it removes one of the equations that need to be satisfied at the equator, specifically

$$\frac{\partial^2 \Psi}{\partial \theta^2}_{i=\frac{N+1}{2}} = 0, \tag{6.21}$$

and is resolved by adding the coupled equations at the equator together to give

$$-\frac{\partial^2 \mathcal{H}}{\partial \theta^2}_{i=\frac{N+1}{2}} + \frac{\partial \Psi}{\partial \theta}_{i=\frac{N+1}{2}} + \frac{\partial^2 \Psi}{\partial \theta^2}_{i=\frac{N+1}{2}} = 0. \tag{6.22}$$

The simplicity of the equations (6.21), (6.22) is due to $\overline{q} = q' = 0$ at this value of latitude and that the spherical scaling in the equations approximate those on a Cartesian co-ordinate system.

As stated previously, an antisymmetric solution in ψ_b enforces a symmetric solution in h_b and there is no need to enforce $^{\partial h_b}$

The coupled system is solved using 2^{nd} order centered differences and 4^{th} order centered differences for the equation at the equator. If 2^{nd} order differences are used throughout, spurious linear solutions are obtained about the equator. The coupled system is described by

$$S_{1,1}\mathbf{x}_1 + S_{1,2}\mathbf{x}_2 = \mathbf{b}_1,$$

for $i = 2$

At the south pole

$$S_{N,N} = \Bigg($$

a 2^{nd} order difference approximation of $\mathcal{H}$ term in equation (6.22). In contrast, the $(1,2)$ entries contain coefficients of a fourth order centred discretisation of the Ψ terms for equation (6.22).

The boundary condition $\Psi = 0$ is enforced by the submatrices A, where

$$A_{\frac{N-1}{2},\frac{N+1}{2}} = \begin{pmatrix} \frac{\cos\theta_{\frac{N-1}{2}+\frac{1}{2}}}{\Delta\theta} & 0 \\ 0 & 0 \end{pmatrix} \qquad A_{\frac{N+3}{2},\frac{N+1}{2}} = \begin{pmatrix} \frac{\cos\theta_{\frac{N+3}{2}-\frac{1}{2}}}{\Delta\theta} & 0 \\ 0 & 0 \end{pmatrix}. \qquad (6.34)$$

6.5 Overall Procedure to obtain balanced / un-

at grid position i, j for the d^{th} dataset. Since the Arawaka C grid is staggered, the position of $\overline{v}_i$ will be $\Delta\theta/2$ away from $\overline{h}_i$ and $\overline{u}_i$

state is subtracted from the perturbations defined by the other datasets to give increments and are denoted using a dash.

The change in control variables needs $\mathcal{Q}'$ and $\overline{q}$ in order to formulate the appropriate right hand side and variable coefficient needed to solve (6.12), (6.13). We apply the DFFT to $\mathcal{Q}'$ to produce the complex coefficients $\tilde{\mathcal{Q}}'$. We rescale the right hand side and $\overline{q}$ to give $2\Omega a^2 cos\theta_i \Delta\theta\tilde{\mathcal{Q}}'$, Q and solve the second order ODE for all wavenumbers using the discretisation presented in Section 6.4. We apply the DIFFT algorithm to $\tilde{\Psi}_i$ and $\widetilde{\mathcal{H}}_i$ and rescale to give h_b and ψ_b.

Three control variables are either chosen from or derived from ψ_b, ψ_{ub}, h_b, h_{ub} and the velocity potential χ. The calculation of the velocity potential of the wind increments (u', v') is described comprehensively in Section 5.5 and Section 5.5.2. The unbalanced height h_{ub} is defined as the difference between h' and h_b.

6.6 Validation Tests

We first apply a 1 dimensional problem to test this coupled system. The base states are chosen to be

$$\begin{aligned} \overline{h} &= \frac{1}{g} \\ \overline{\psi} &= 0 \\ \overline{q} &= 2g\omega \sin\theta \end{aligned} \tag{6.39}$$

with the scaled potential vorticity increment being,

$$q' = -\frac{2g^2 \sin\theta}{a^2} + g^2\omega^2 \sin\theta \left(\cos 2\theta - \frac{1}{3}\right) \tag{6.40}$$

so that the analytic balanced streamfunction ψ_b and balanced height are given by

$$\begin{aligned} \psi_b &= g \sin\theta \\ h_b &= -\frac{\omega \cos 2\theta}{2} + \frac{\omega}{6}. \end{aligned} \tag{6.41}$$

This is a good problem which examines the longitudinally independent part of a general solution to the 2 dimensional problem, for the Fourier coefficents relating to $k = 0$.

In Figure 6.1 we show the error profile between the analytic solutions and the experimental results, when ($N = 33, 65, 129$) across latitudes. The error in the balanced height is slightly larger at the equator than elsewhere. This is expected due to the need to solve equation (6.22) with finite differencing (6.33). In contrast, the error in the streamfunction is the most at the poles. The decrease in error with increasing resolution moves to 2^{nd} order accuracy as the resolution is increased, as shown in Tables 6.1, 6.2. Table 6.1 shows the decrease in error in the balanced height and streamfunction, where the error for each considered, is taken as the L_2 vector norm of the error at each latitudinal point, divided by . The order of accuracy is given in Table 6.2.

The 'coupled system' method is tested using full height and wind fields, $h, \mathbf{v}$, which satisfy a Rossby Haurwitz wave (3.36), (3.34) with parameters $R = 4$, $K = \omega = 7.848 \times 10^{-7} s^{-1}$ and $h_0 = 8000m$. The linearisation states are defined to be about a resting state $\overline{\mathbf{v}} = 0$ and a constant height field $\overline{h} = 8000m$. The base state perturbation is also defined to be stationary with a constant height field h_{base} chosen such that the surface integral of this quantity is equal to the surface integral of $h - \overline{h}$. Thus the full increment is defined by $R = 4$, $K = \omega = 7.848 \times 10^{-7} s^{-1}$ and

Figure 6.1: Error in balanced streamfunction and height across various latitudes and resolutions

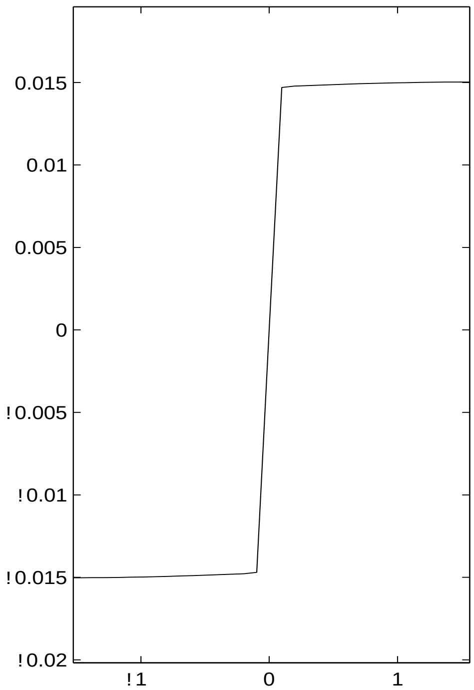

Figure 6.2: Full height increment (left) and full streamfunction increment (right) in a Rossby Haurwitz increment $K = 7.848 \times 10^{-7} s^{-1}$, $h_0 = -h_{base}$ and $R = 4$ with linearisation and base states $\overline{h} = 8000\ m$, $\overline{u} = 0$, $\overline{v} = 0$

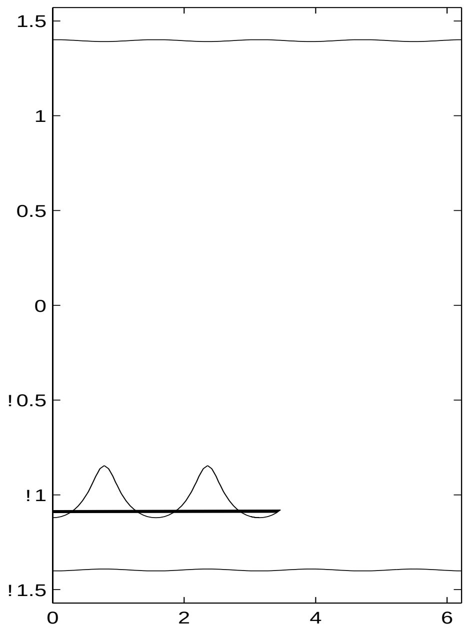

Figure 6.4: F

Figure 6.6: Error between balanced height increments derived from LBE using ψ_b from Figure 6.3 and from the coupled system for M=96 and N=65

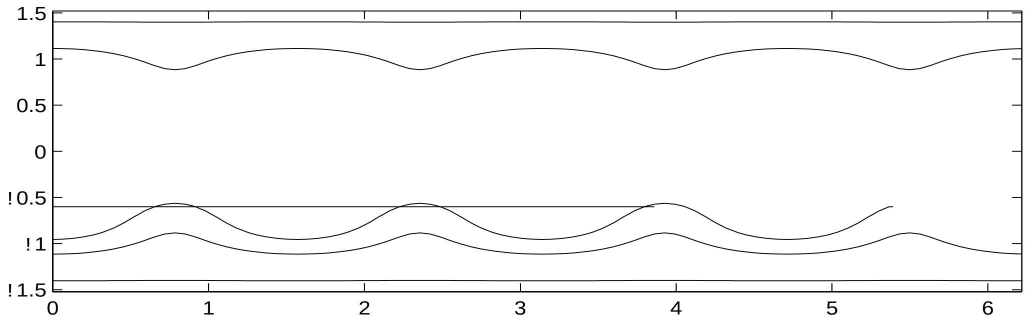

Table 6.3: (top)L_2 error in h_b, divided by $(N-2)+2$, under different resolutions, (bottom) order of convergence of h_b under different resolutions

N	M	L_2 difference in balanced height using coupled system
33	48	2.81×10^{-1}
65	96	3.20×10^{-2}
129	192	7.27×10^{-3}

N	M	
$65-33$	$96-48$	3.13
$129-65$	$192-96$	2.14

and the difference between this field and $\mathcal{Q}'$ obtained by applying a second order discrete Laplacian operator to ψ_b and subtracting $\overline{q}h_b$. We see that at this resolution the computed error is approximately a hundredth of the value of the original field.

Table 6.6 shows a similar decrease in the difference of these fields with increasing grid resolution. In this table, the discrete integral L_2 norm is used, whose form is given by

$$\mathcal{Q}'_{err} = \sqrt{\Big(\sum_{i=1}^{i=N}\sum_{j=1}^{j=M}\left(\frac{V_i \mathcal{Q}'_{diff\ i,j}}{\quad}\right)^2}. \tag{6.42}$$

where V_i is defined in equation (6.9), $\mathcal{Q}'_{diff}$ is the difference between the the full increment and balanced increment evaluations of $\mathcal{Q}'$ at grid position i, j.

Figure 6.7: (left) $\mathcal{Q}'$ as calculated from the full increments; (right) error in $\mathcal{Q}'$, derived from full increments and from balanced increments

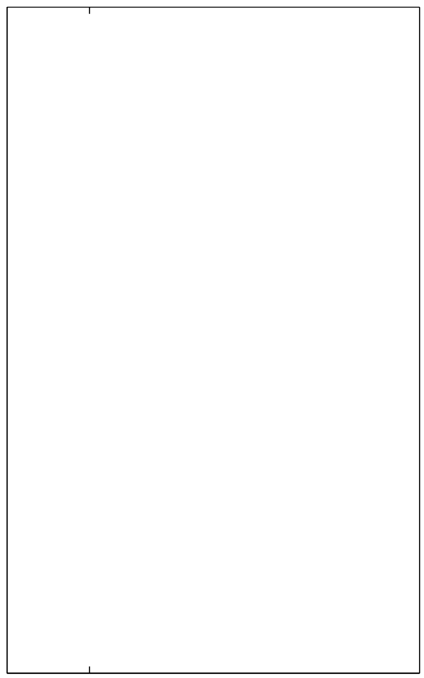

6.7 The inverse transform

In this section we describe the opposite transformation from old and new control variables to the associated wind and height fields. In Chapter 4, various changes into and out of control variables are discussed. The changes out of control variables into height and wind fields use at some point variants of a simple Helmholtz decomposition (5.40). The numerical details of the decomposition are already giv

Table 6.5: Discrete L_2 integral error in U and V under different resolutions

N	M	L_2 error in U	L_2 error in V
33	48	2.39×10^{-2}	7.02×10^{-2}
65	96	3.08×10^{-3}	9.07×10^{-3}
129	192	3.89×10^{-4}	1.14×10^{-3}

N	M	Order accuracy in U	Order accuracy in V
$65 - 33$	$96 - 48$	2.96	2.96
$129 - 65$	$192 - 96$	2.99	2.99

for both LB and PV methods. We use divergence tendency as an indicator as to how 'balanced' the balanced control variables are. A small value indicates good performance. Two experiments are performed; one with the balanced Rossby Haurwitz wave and the other with unbalanced increments. The experiment with the Rossby–Haurwitz wave shows slightly worse results in the low Burger number. The experiment using unbalanced increments shows that the PV method produces the lowest divergence tendency when applied to the original Burger regime from which the increments originate. In this regime it is doing better than the LB method. However the PV method is performing slightly worse in low Burger regimes. This may be due to the method trying to approximate full unbalanced height increments.

7. Experiment 1: Relative Contribution of Height and Absolute Vorticity to Potential Vorticity

We want to show the linearised potential vorticity perturbation captures the dynamical flow over different regimes.

In Section 3.9 we show that the scaled height

$$\vartheta = -\frac{h^*}{\overline{h}} \tag{7.1}$$

and scaled vorticity

$$\iota = \frac{\zeta^*}{\overline{\zeta}} \tag{7.2}$$

contribute to the scaled potential vorticity

$$\kappa = \frac{q^*}{\overline{q}} \tag{7.3}$$

in such a way that is dependent on the Burger number (3.5) : for a high Burger regime, ι contributes most towards κ, while for low Burger regimes the ϑ is the dominant part of κ. Since the theory is carried out on an f-plane, it is prudent to perform an experiment to see whether the theory is satisfied in practice within a more general setting where the Coriolis parameter that varies with latitude.

The full velocit

Burger number is larger than 1 for all latitudes considered. Thus we identify: the wave with parameters $h_0 = 50m$, $K = \omega = 7.848 \times 10^{-7}\ s^{-1}$ as representing a low Burger regime, the wave with parameters $h_0 = 8000\ m$, $K = \omega = 7.848 \times 10^{-7}\ s^{-1}$ representing a high Burger regime, and the rest in between representing a mixture of high and low Burger regimes dependent on latitude.

Figure 7.1: Burger values at different latitudes and h_0 when $K = 7.848 \times 10^{-7}\ s^{-1}$ (left), $K = 7.848 \times 10^{-6}\ s^{-1}$ (right)

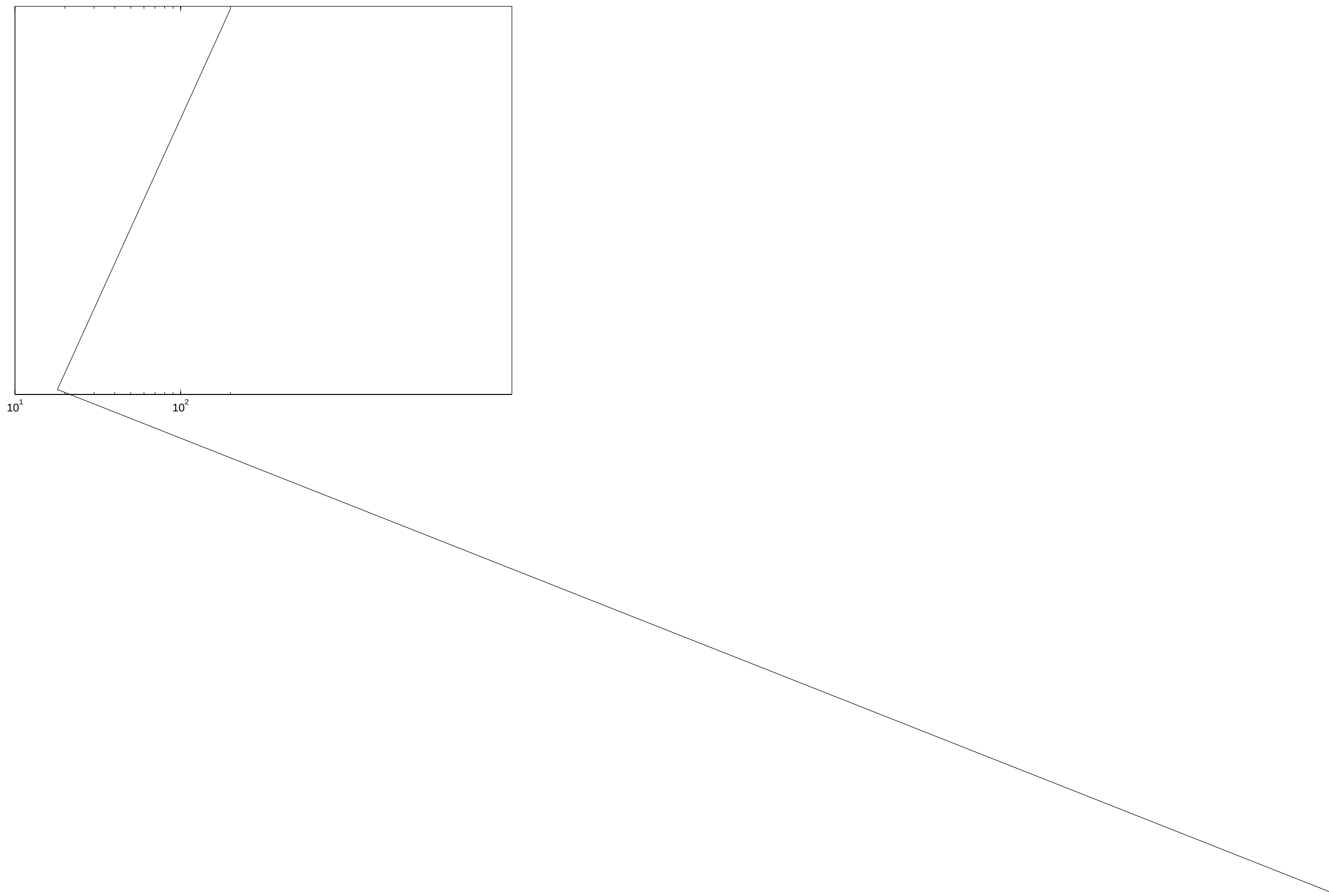

contribution ι is similar in size to the scaled potential vorticity perturbation κ.

Conversely

Example 1: $h_0 = 8000\ m$, $\omega = K = 7.847 \times 10^{-7}\ s^{-1}$ **(Figure 7.4)**

In this high Burger regime the height field for the most part keeps the shape of its initial condition; the whole wav

$7.848 \times 10^{-6}\ s^{-1}$.

perturbations. Experiment 1 also concurs with this finding. In Experiment 2 we have shown that for small Burger numbers, the height fields contribute more strongly to the potential vorticity. For Burger numbers larger than 1, the greater contribution to the potential vorticity comes from the absolute vorticity, an example of which occurs when $h_0 = 8000\ m$. In this region the potential vorticity mirrors the absolute vorticity field. However there is a loss in detail in these regions. When vortices are produced in the mid-latitudes, they involve sharp changes in velocity and a substantial decrease in the characteristic length scale. The smaller characteristic length scale results in the formation of a high Burger number regime. Again, the absolute vorticity resembles the potential vorticity more accurately than the height. However, the potential vorticity field is less detailed than the absolute vorticity. Hence the theory developed in Section 3.9 for the f-plane appears to hold on the sphere.

7.3 Comparsion of balanced with full fields at high and low Burger number

In order to investigate whether the coupled system of equations provides a better representation of balanced and unbalanced control variables it is necessary to

Figure 7.3: Relative contributions of the absolute vorticity ι and height ϑ to the potential vorticity κ for $K = 7.848 \times 10^{-6}\ s^{-1}$ with different latitudes and h_0. Sensitivity is defined by the magnitude of the scaled perturbation in question

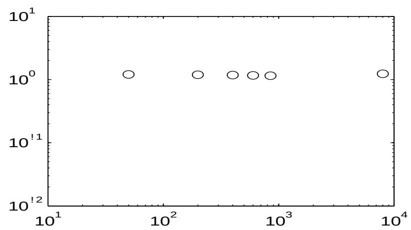

Figure 7.5: Potential vorticity, Absolute vorticity and height fields when $K = 7.848 \times 10^{-7} s^{-1}$ and $h_0 = 50\ m$ after 2 days

height perturbations contribute more to the potential vorticity perturbations. If the coupled system is behaving properly, then in high Burger regimes the streamfunction ψ should be similar to the balanced streamfunction ψ_b. Similarly, at low Burger regimes the balanced height should resemble the full height field. A Rossby Haurwitz wave (3.34), (3.35), (3.36) (RH wave) is used as an initial condition to a global SWE (2.37), (2.36) model. The defining parameters are $R = 4$, $K = \omega = 7.847e^{-7}s^{-1}, h_0 = 8000m$. Such values produce a high Burger regime across the whole globe, with the Burger number, $B_u = 1.78$ at $60°\theta$, $B_u = 1.55$ at $45°\theta$ and $B_u = 4.55$ at $10°\theta$. The global SWE model was run for 24 hrs, with a timestep of 0.5 hr at medium spatial resolution with grid spacing $\Delta\theta = \pi/64$, and $\Delta\lambda = \pi/48$. The coupled balanced method was used to produce balanced height and streamfunction by applying the procedure detailed in Section 6.5 and excluding the final calculation of increments. Figure 7.7 compares the balanced streamfunction to the respective full field over the area $[(\theta \in [\pi/2, -\pi/2]) \times (\lambda \in [0, \pi/2])]$.

Figure 7.7: Balanced ψ (left) and full ψ (right) for RH wave propagated 1 day at high Burger number, for $(\theta \in [\pi/2, -\pi/2]) \times (\lambda \in [0, \pi/2])$ (scale denotes grid points)

Figure 7.10: Balanced height (left) and full height (right) for RH wave propagated 1 day at low Burger number, with $(\theta \in [\pi/2, -\pi/2]) \times (\lambda \in [0, \pi/2])$ (scale denotes grid points)

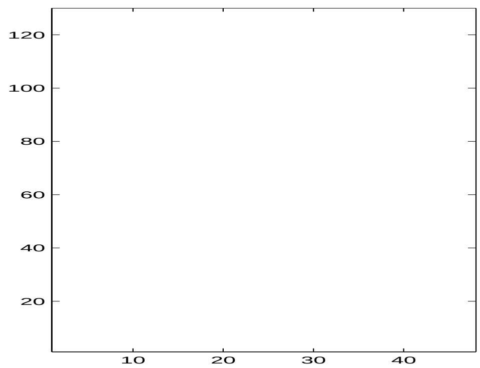

vary between $-60m$ and $60m$. It is also clear from the figure that there is great variability in the flow with waves of both short and long wavelengths present.

If the initialisation is perfect then the increments consist of just the unbalanced flow. A perfect set of control variables would apportion the flow into the t

Figure 7.11: (Top) U and V wind increments produced using test case $INI7C$, (bottom right) height increment using test case $INI7C$, (bottom left) U field linearisation state

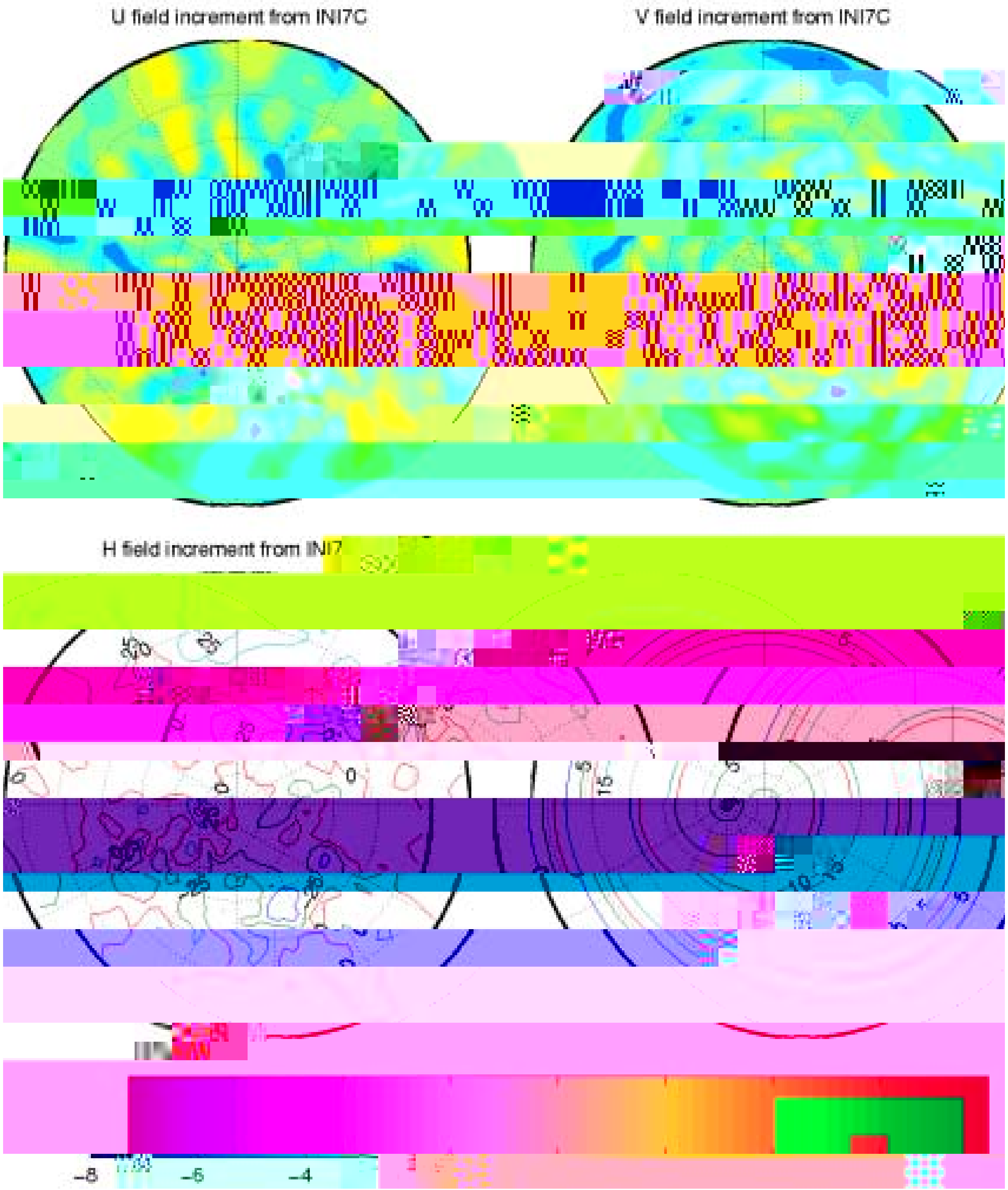

somewhat surprising. The balanced winds from the two methods are dissimilar. The balanced winds from the PV method are much smaller. This is because the scaled potential vorticity increment $\overline{h}q'$ does not resemble the full vorticity increment ζ'. There is cancellation between ζ' and $\overline{q}h$ as they are of the small magnitude throughout the fields. This makes the scaled linearised potential vorticity increments $\overline{h}q'$ a factor of ten smaller than the vorticity increment ζ'. This also shows that the PV method is performing better than the LB method at producing balanced fields.

To check that the balanced wind produced by the PV method moves towards the balanced wind from the LB method when Burger number is increased, we choose a mean height of $101km$. We see that in Figure 7.16 the balanced winds from the two methods are quantitively similar; the U component of the balanced wind is positive about the pole and swaps direction in the mid-latitudes. In the low Burger regime the balanced wind increments produced by the PV method are more pronounced due to the balanced height increment approaching the full height increment. This is readily seen in Figures 7.15 and 7.13.

The theory presented in Sections 3.9, 4.7 concur with these findings. However they presume that for low Burger regimes the full height increments represents the balance in the system and that the vorticity is the key balanced variable when the Burger number is large. However in this experiment both the full height and wind increments are unbalanced. When the PV method is at very high Burger number, the scaled potential vorticity increment represents the full unbalanced vorticity increment. Conversely, at low Burger regimes the scaled potential vorticity increment resembles the full unbalanced height increment.

It is interesting to note that around the equator, the LB and PV methods are not producing similar results even though a high Burger regime is always present

Similar findings are found in the balanced correction to the departure from linear balance. The L_2 vector norm is also used to compare the different increments. We describe this correction in terms of a streamfunction and see that the LB method gives a value of 3.4×10^6 m^2s^{-1} . Again the PV method has a smaller value of 2.3×10^5 m^2s^{-1} at high Burger number. In contrast, at low Burger number the PV method produces a larger value of 1.8×10^7 m^2s^{-1}.

This section supports much of the theory given in Sections 3.9, 4.7. The experiments with RH wave have shown that the balanced height and wind produced by the PV method vary with Burger number as expected. The application of unbalanced increments to both methods shows the importance in how increments are generated. The PV method at low Burger number produces ‘balanced’ increments that are similar to the full increments, even when the full increments are ‘unbalanced’. We have shown that at high Burger number the PV method is performing better than the LB method, with there being far less balanced flow found in the control variables. At low Burger number the balanced divergence obtained from the PV and LB method are of the same order of magnitude.

7.4 Divergence Tendency

The divergence tendency is a good measure with which to compare different sets of control variables. Ideally, we wish the divergence tendency of a set of variables to be small. The first series of experiments we present considers only the divergence tendency of the balanceddtheTJ!“balanie“TD!Tc!“TD!shoTj!tBlrtendecmparedTD!‘Tc!t(ishnd!.‘m in magnitude to the present version.

We choose extreme examples of the RH wave at high and low Burger regimes to provide the full fields. The high Burger regime is determined by choosing the defining parameters to be ($h_0 = 8000\ m$, $K = \omega = 7.686 \times 10^{-7}\ s^{-1}$) and giving a Burger number of approximately 1.55 at $\theta = 45°$. The low Burger regime uses ($h_0 = 0\ m$, $K = \omega = 7.686 \times 10^{-7}\ s^{-1}$) and has $B_u \approx 0.30$ at $\theta = 45°$. The RH wave is by definition in Charney balance and has a divergence tendency of zero. When the LB and PV methods are applied to the RH wave, the divergence tendency from the balanced variables is no longer zero but given by (4.53), (4.54). As the winds of the RH wave are rotational the LB method considers the full wind perturbation as balanced. The divergence tendency in this case is just equal to minus the divergence of the advective term of the shallow water momentum equations.

We apply the PV method to calculate perturbations about a resting state and a constant height H using the full height and winds from the high Burger regime which we describe in Section 5.4 and equations (5.2), (5.3). The corresponding low Burger regime is produced by only changing the value of the constant height H. The height and wind perturbations are kept the same as in the high Burger regime. The value of H in the low Burger regime is chosen such that the sum of the height perturbation and H gives a value of zero about the poles. This is done so that the full height field is non-negative. Also keeping the perturbations and the other linearisation states the same allows comparisons to be made easily.

In the high Burger regime the balanced wind perturbations from the PV method approximate the full perturbations. Since the divergence tendency is determined solely from the balanced winds, we expect the divergence tendencies to be similar.

This is clearly seen in Figure 7.17 where the L_2 norm of the divergence tendencies about each latitude ring is given. The results from the LB and PV methods at high Burger number are denoted by circles and crosses, respectively.

In the low Burger regime the divergence tendency from the LB method remains unchanged as the rotational wind perturbation is not varied with Burger number. The results from the PV method do change. The norm of the divergence tendencies of the PV method are noticably worse around the equator in between $\theta = 0°$ and $\theta = 10°$. This may be due to a possible inconsistency between the linearised potential vorticity perturbation and its associated balance condition. This could be rectified by using a balance condition which is more applicable to the tropics. In the mid-latitudes the results from the PV method are mixed. There are regions within the mid-latitudes in which the PV method is performing better. Likewise there are regions where LB method is superior. Overall the PV method may be performing slightly worse than the LB method. However the differences between the two methods are small with the div

So far we have considered only the divergence tendency of balanced variables from LB and PV methods when the initial field field is in Charney balance. We wish to consider increments derived from subtracting the uninitialised fields in data set *VDG7.13.cdf* from the respective initialised fields and calculate overall divergence tendencies for high and low Burger number. In particular we present the L_2 norm of the linearised divergence tendency increments for not only the balanced control variables but also the balanced corrections to the control variables. The linearised divergence tendencies are as defined in equations (4.53),(4.54), (4.71), (4.72). They are approximated using second order centered finite differences. The remaining experimental details are the same as in Section 7.3.

Table 7.1 shows the L_2 vector norm of the linearised divergence tendencies increment of the balanced control variable increments and balanced corrections to unbalanced control variables. We see that the PV method at high Burger number performs the best for balanced control variable increments and balanced corrections to unbalanced control variables. If the PV method is set at even higher Burger numbers, the divergence tendencies would move to those given by the LB method. For low Burger number the PV method gives the divergence tendencies that are significantly worse. This is due to the method approximating the full unbalanced height increments.

In conclusion, we see that a regime dependent set of control variables given by the PV method gives overall results that are promising. Sections 7.2, 7.2.1 show the relationship between scaled potential vorticity, height and absolute vorticity perturbations at different Burger regimes for a Rossby-Haurwitz wave. Section 7.3 has shown that the PV method behaves as expected y-fhe an

Table 7.1: L_2 v

used; in high Burger regimes it is approximating the solution given by using the LB method and at low Burger number the balanced height is determined by the height perturbation. When unbalanced increments are used in a high Burger regime the PV method performs better than the LB method. We then perform two experiments considering the divergence tendencies of the control variables. The experiment with the RH wave shows slightly worse results in the low Burger number. The experiment using unbalanced increments, shows that the PV method produces the lowest divergence tendency when applied to the original Burger regime from which the increments originate. The PV method is better in this situation at capturing the unbalanced part of the flow. However the PV method works slightly worse than expected when the same increments are introduced into different regime. However it still remains to be seen whether the PV method will perform better with height and wind increments that are mainly balanced and also have a small unbalanced part.

Figure 7.12: H field linearisation states for low Burger regime (left) and high Burger regime (right)

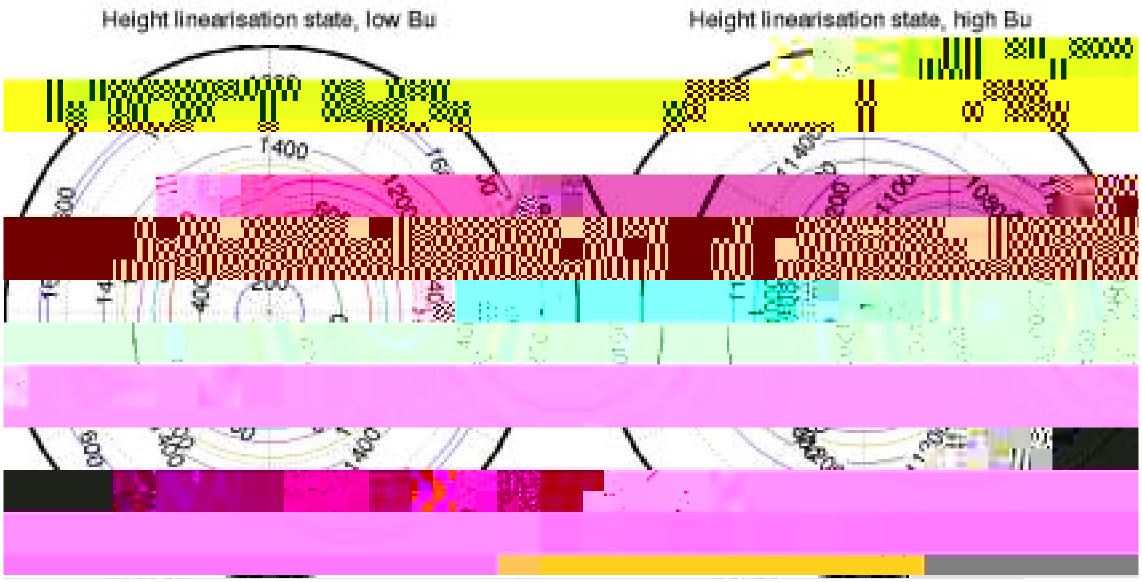

Figure 7.13: (Top left) Height increment produced using test case $INI7C$. (Top right) balanced height increment produced by LB method. (Bottom left) Balanced height increment using PV method at low Bu. (Bottom right) Balanced height increment using PV method at high Bu

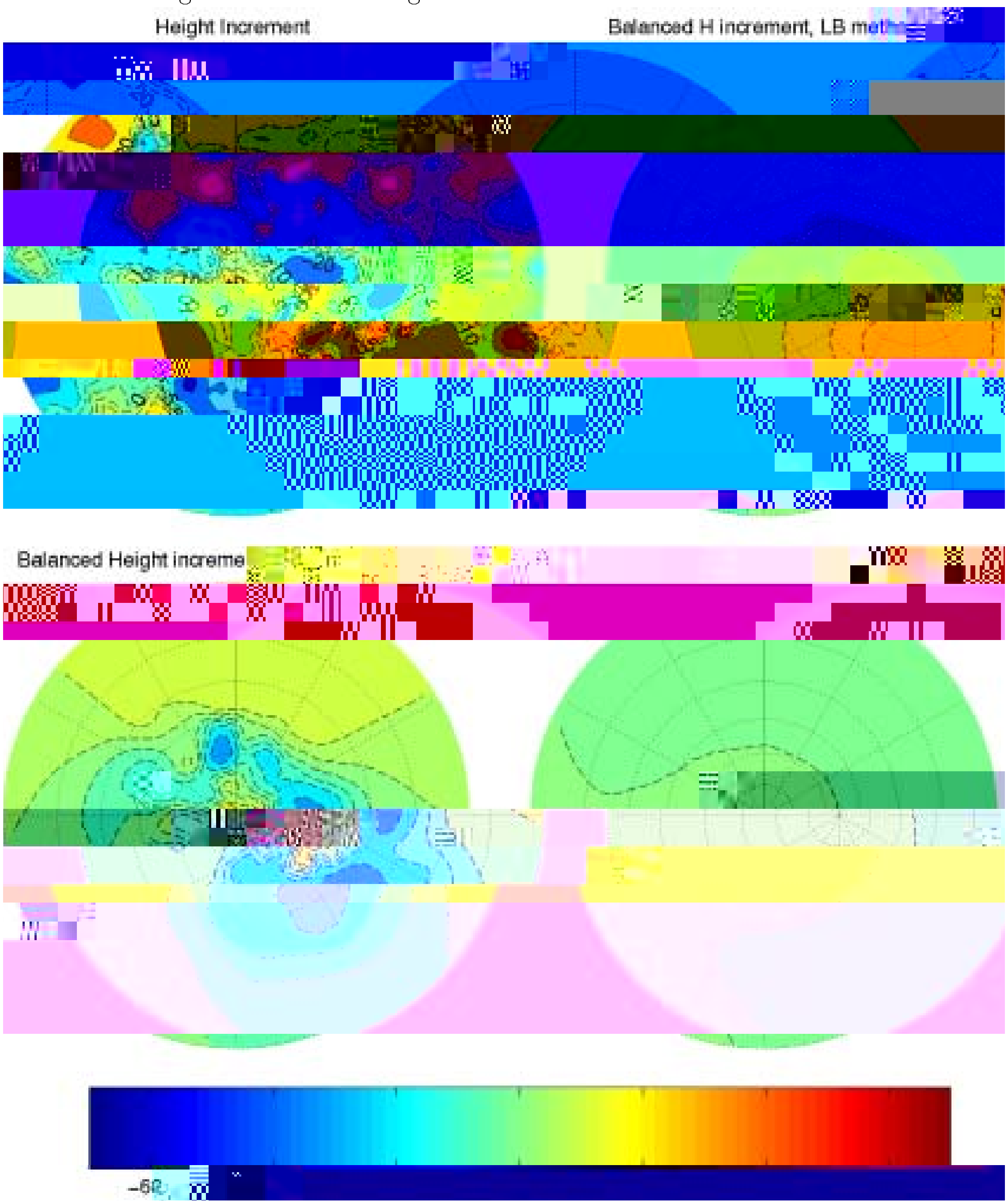

Figure 7.14: Balanced wind increments produced by using the LB and PV methods at high Bu (mean height $H \approx 11km$)

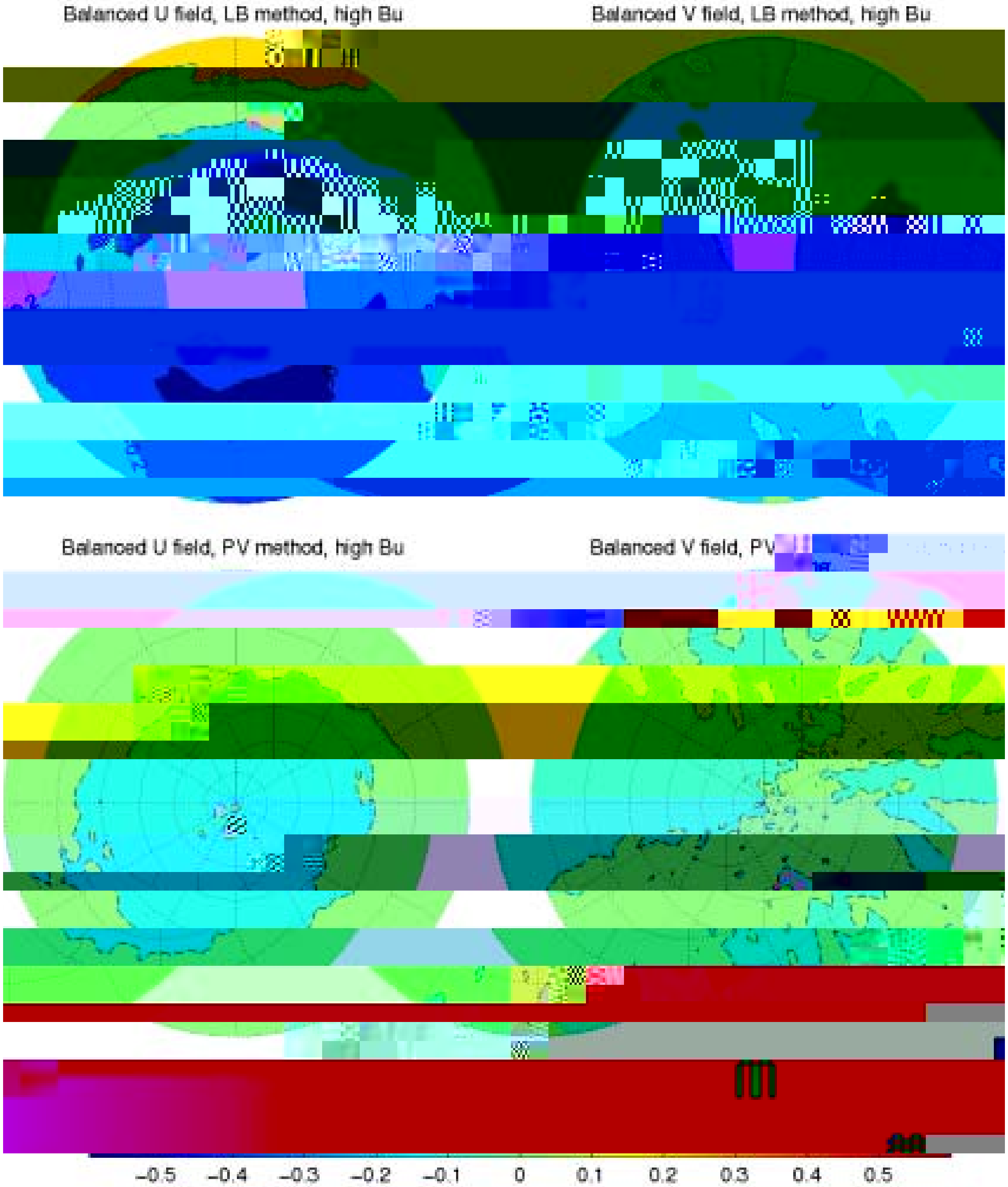

Figure 7.15: Balanced wind increments produced by using the LB and PV methods

Figure 7.16: Balanced wind increments produced by using the LB and PV methods at very hi Bu (mean height $H \approx 100km$), (latitudinally varying linearisation states)

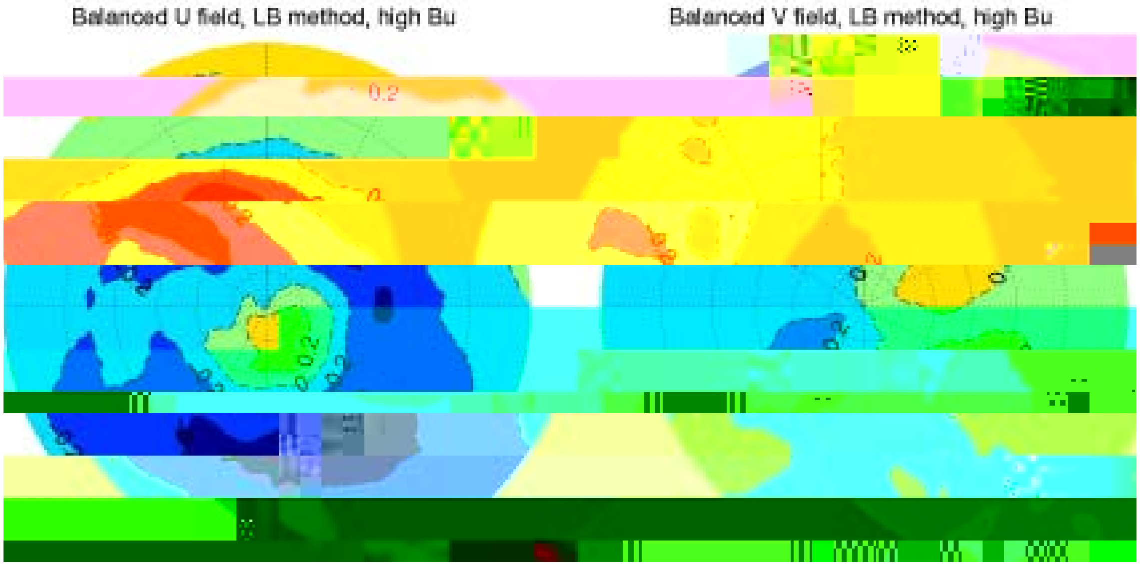

Figure 7.17: L_2 norm of divergence tendencies RH waves at high and low Bu using PV and LB methods

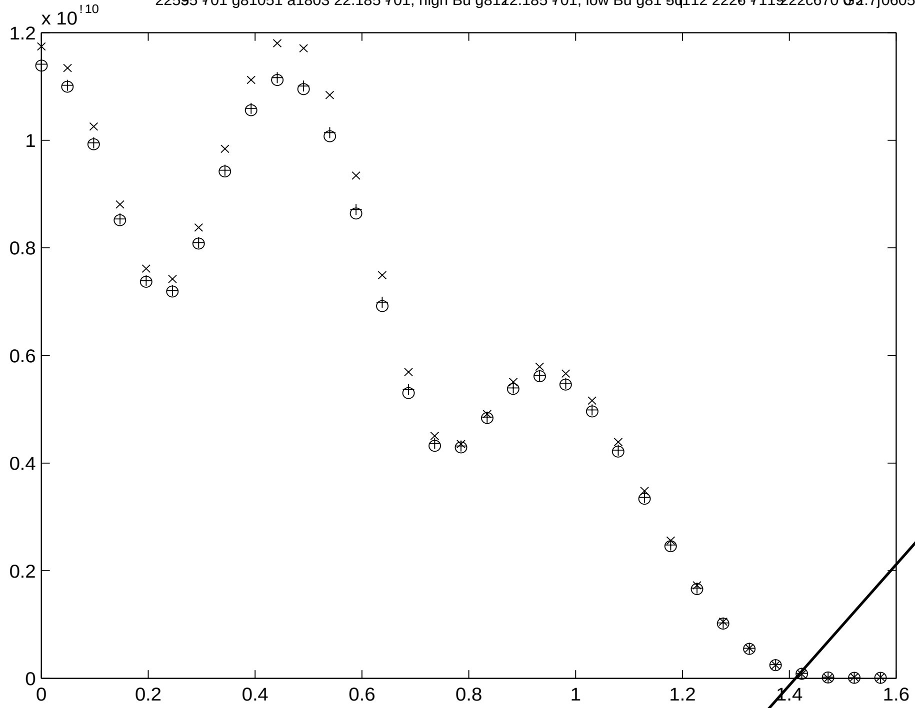

hapter 8

onclusion

Throughout this thesis we have considered the use of potential vorticity as a control variable. To this end in Chapter 3 we have given a clear mathematical description of balance. A number of issues have come to light that tend to get forgotten. Setting the divergence tendency to zero eliminates the unbalanced inertio-gravity waves only when we consider the f-plane SWEs linearised about a resting state. F

method will approximate a height constrained set of control variables described by (4.73) and (4.74).

The experimen

8.1 Further ork

More experiments need to be performed in order to be certain that the potential vorticity-based set of control variables is better than the current method. One way would be to apply the method to height and wind increments generated using the NMC method ([41]), ([29]) from a multi-layered barotropic model approximating the atmosphere. As the full increments should be predominantly balanced, the PV method should produce smaller divergence tendencies in the balanced control variable than the LB method.

Obtaining the balanced control variable of the PV method is essentially a 'poor man's' version of the 1st order direct potential vorticity inverter described by McIntyre [36]. Instead of using a Charney balance condition, the LBE is used instead. It would be interesting to use the Charney balance condition instead and compare the results. This should be not difficult to achieve as it would need minor changes to be applied to the code used to produce balanced corrections to the departure from linear balance. A linearisation of the Charney balance equation about latitudinally varying states would be used. The coupled system to be solved on a hemisphere is

$$\begin{aligned} -\nabla \cdot \left(f + \overline{\zeta}\right) \nabla \psi_b - \mathbf{k} \cdot \nabla \times \left(\nabla^2 \psi_b \overline{\mathbf{v}}\right) & \\ + g\nabla^2 h_b + \nabla^2 \left(\overline{\mathbf{v}} \cdot \left(\mathbf{k} \times \nabla \psi_b\right)\right) &= 0, \\ \nabla^2 \psi_b - \overline{q} h_b &= \nabla^2 \psi' - \overline{q} h', \end{aligned} \tag{8.1}$$

where the boundary conditions are the same as those used in the PV method.

So far we have considered the control variable transformations on a hemisphere. To consider the control variable transformations in a more realistic context we need to generalise the work for flows whose variables are neither symmetric nor antisymmetric about the equator. If we use the same technique as before, we would need four equations and four variables. In addition to solving for only symmetric height and an antisymmetric streamfunction we would need to evaluate an antisymmetric height field and a symmetric streamfunction. In principle this can be achieved by solving the system

$$\nabla \cdot f\nabla\psi_a - g\nabla^2 h_s = 0 \tag{8.2}$$

$$\nabla^2\psi_a - \overline{q}_a h_s - \overline{q}_s h_a = \nabla^2\psi_a' - \overline{q}_a h_s' - \overline{q}_s h_a' \tag{8.3}$$

$$\nabla \cdot f\nabla\psi_s - g\nabla^2 h_a = 0 \tag{8.4}$$

$$-\overline{q}_a h_s + \nabla^2\psi_s - \overline{q}_s h_a = \nabla^2\psi_s' - \overline{q}_s h_s' - \overline{q}_a h_a' \tag{8.5}$$

simultaneously, where ψ_a and h_a are the balanced height and streamfunction parts which are antisymmetric about the equator, ψ_s

divergence tendency and the second order partial time derivative of the balanced divergence to zero. This method gives a time invariant balanced divergence. In the third order direct inversion the second and third order partial time derivatives of the balanced divergence are set to zero. This would allow a time varying balanced divergence to be obtained. The use of this third order inversion would accurately represent key dynamical features present in the tropics. It would also be the limit in which potential vorticity inversion is useful [18].

References

[1] F. Baer. The spectral balance equation. *Tellus*, 29:107–115, 1977.

[2] S.R.M. Barros. Multigrid methods for two- and three-dimensional Poisson-type equations on the sphere. *J. Comput. Phys.*, 92:313–348, 1991.

[3] J.R. Bates, Y. Li, A. Brandt, S.F. McCormick, and Ruge. A global shallow-water numerical model based on the semi-lagrangian adv

[8] J. Charney. The use of the primitive equations of motion in numerical predic-

2000.

[19] M. Frigo and S.G. Johnson. FFTW (http://www.fftw.org).

[20] M. Frigo and S.G. Johnson. FFTW: An adaptive software architecture for the FFT. *Proceedings of the International Conference on Acoustic, Speech, and Signal Processing*, 3:1381–1384, 1998.

[21] P.R. Gent. Balanced models in isentropic coordinates and the shallow water equations. *TellusA*, 36A:166–171, 1984.

[22] A. E. Gill. *Atmosphere-Ocean Press.* Academic Press, 1982.

[23] Haltiner and Williams. *Numerical Prediction and ynamical Meteorology.* Wiley, 2 edition, 1980.

[24] Haurwitz. *Compendium of Meteorology*, chapter The Perturbation Equations of the Atmosphere, pages 416–417. AMS, 1951.

[25] R. Heikes and D.A.Randall. The shallow water equations on a spherical geodesic grid. Technical Report 524, Department of Atmospheric Science, 1993.

[26] J.R Holton. *An Introduction to ynamic Meteorology.* Academic Press Inc., second edition, 1979.

[27] B.J. Hoskins. Stability of the Rossby-Haurwitz wave. *uart. J. R. Met. Soc.*, 99:723–745, 1973.t o S o . R . a

[29] N.B. Ingleby. The statistical structure of forecast errors and its representation in The Met. Office Global Variational Data Assimilation Scheme. *uart. J. R. Met. Soc.*, 571A:209–222, 2001.

[30] R. Jacob, J. Hack, and D. Williamson. Solutions to the shallow water test set using the spectral transform method. Technical report, NCAR, 1993.

[31] A.C. Lorenc. Analysis methods for numerical weather predition. *uart. J. R. Met. Soc.*, 111:1777–1194, 1986.

[32] A.C. Lorenc, S.B. Ballard, R.S. Bell, N.B. Ingleby, P.L. Andrews, D.M. Barker,

[37] P

[48] C G Rossby and collaborators. Relation between variations in the intensity of the zonal circulation of the atmosphere and the displacements of the semi-permanent centers of action. *Journal of Marine Research*, 2:38–55, 1939.

[49] I. Roulstone and M.J. Sewell. The mathematical structure of theories of semi-geostrophic type. *Phil. Trans. R. Soc. Lond.*, A355:2489–2517, 1997.

[50] A.L. Schoenstadt. The effect of spatial discretisation on the steady state and transient behaviour of a dispersive wave equation. *J. Comp. Physics*, pages 364–379, 1977.

[51] J.G. Smith and A.J.Duncan. *Elementary Statistics and Applications: Fundamentals of the theory of statistics*. McGraw-Hill, 1944.

[52] P.N. Swarztrauber. The direct solution of the discrete Poisson equation on the surface of a sphere. *J. Comp. Phys.*, 1974.

[53] C. Temperton. Implicit normal mode initialisation. *Mon. Wea. Rev.*, 116:1013–

[57] Eric W. Weisstein. *CRC Concise Encyclopedia of Mathematics*. CRC Press, 1998.

[58] A. White. A view of the equations of meteorological dynamics and various approximations. Technical report, The Met. Office, 2000.

[59] D.L. Williamson and J.B. Drake. A standard test set for numerical approximations to the shallow water equations in spherical geometry. *J. Comp. Phys.*, 102:211–224, 1992.

[60] A. Winn-Nielsen. On geostrophic adjustment on the sphere. *Beit. Phys. Atmos.*, 49:254–271, 1976.